

Review

Combining Passive Infrared and Microwave Satellite Observations to Investigate Cloud Microphysical Properties: A Review

Mariassunta Viggiano ¹, Domenico Cimini ^{1,2}, Maria Pia De Natale ¹, Francesco Di Paola ¹,
Donatello Gallucci ¹, Salvatore Larosa ¹, Davide Marro ¹, Saverio Teodosio Nilo ^{1,*} and Filomena Romano ¹

- ¹ National Research Council of Italy, Institute of Methodologies for Environmental Analysis, (CNR-IMAA), 85050 Tito, Italy; mariassunta.viggiano@cnr.it (M.V.); domenico.cimini@cnr.it (D.C.); mariapia.denatale@cnr.it (M.P.D.N.); francesco.dipaola@cnr.it (F.D.P.); donatello.gallucci@cnr.it (D.G.); salvatore-larosa@cnr.it (S.L.); davide.marro@studio.unibo.it (D.M.); filomena.romano@cnr.it (F.R.)
- ² Center of Excellence Telesensing of Environment and Model Prediction of Severe Events (CETEMPS), Università dell'Aquila, 67100 L'Aquila, Italy
- * Correspondence: saverioteodosio.nilo@cnr.it

Abstract: Clouds play a key role in the Earth's radiation budget, weather, and hydrological cycle, as well as the radiative and thermodynamic components of the climate system. Spaceborne observations are an essential tool to detect clouds, study cloud–radiation interactions, and explore their microphysical properties. Recent advancements in spatial, spectral, and temporal resolutions of satellite-borne measurements and the increasing variety of orbits and observing geometries offer the opportunity for more efficient and sophisticated retrieval procedures, leading to the more accurate estimation of cloud parameters. However, despite the availability of near-coincident observations of the same atmospheric state, the synergy between the whole set of acquired information is still largely underexplored. The use of synergy is often invoked to optimize the exploitation of the available information, but it is rarely implemented. Indeed, the strategy currently used in most cases is that retrievals are performed separately for each instrument and, only later, the retrieved products are combined. In this framework, therefore, there is a strong need to study and exploit the synergy potential of the instruments currently in orbit or that will be put in orbit in the next few years. This paper reviews the efforts already made in this direction, combining passive infrared and microwave to retrieve cloud microphysical properties. We provide readers with a framework to interpret the state of the art, highlighting the pros and cons of the various approaches currently used with a look to the most promising methodologies to be deployed to address the challenges of this field.

Keywords: satellite observations; cloud properties; infrared; microwave



Academic Editor: Gang Zheng

Received: 29 November 2024

Revised: 16 January 2025

Accepted: 17 January 2025

Published: 19 January 2025

Citation: Viggiano, M.; Cimini, D.; De Natale, M.P.; Di Paola, F.; Gallucci, D.; Larosa, S.; Marro, D.; Nilo, S.T.; Romano, F. Combining Passive Infrared and Microwave Satellite Observations to Investigate Cloud Microphysical Properties: A Review. *Remote Sens.* **2025**, *17*, 337. <https://doi.org/10.3390/rs17020337>

Copyright: © 2025 by the authors. Licensee MDPI, Basel, Switzerland. This article is an open access article distributed under the terms and conditions of the Creative Commons Attribution (CC BY) license (<https://creativecommons.org/licenses/by/4.0/>).

1. Introduction

Among the many factors influencing climate change, clouds occupy a first-order position due to the high degree of uncertainty they bring, as stated by the Intergovernmental Panel on Climate Change (IPCC) in the sixth Assessment Report (AR6) [1]. Furthermore, understanding clouds and climate circulation and their implications for forecasting extreme meteorological events is included among the World Climate Research Program's grand challenges (<http://wcrp-climate.org/grand-challenges> (accessed on 18 January 2025)) to be addressed in the next decade. In addition, given the key role of clouds in moisture redistribution and the hydrological cycle, advances in the field of atmospheric science

cannot occur without real progress in understanding cloud-scale microphysical variables. For these reasons, numerous efforts have been made in recent years to deepen the knowledge of global cloud distribution and develop and improve the accuracy of methodologies that estimate key microphysical cloud variables. Although satellite observations currently offer a complete view of the entire Earth's surface for both the frequency and geographic distribution of the observations, as well as for their spectral range (from VIS to MW), and despite the high quality level achieved in the field of radiative transfer modeling, the accuracy in retrieving key cloud microphysical variables is not always satisfactory. The results of the most recent works seem to indicate that a significant contribution in this sense can come from the synergic use of information from different frequencies. However, today, retrieval products typically come from separate observations at microwave (MW) and infrared (IR) frequencies, which are combined only later, as illustrated in Figure 1. In this way, the synergy potential between these observations is not fully exploited. Conversely, algorithms should simultaneously/hierarchically combine all complementary information derived from different spectral ranges, thus achieving more accurate retrievals than independent retrievals combined a posteriori. In fact, MW is complementary to IR observations, especially in cloudy situations. This is due to relatively low cloud opacity and, therefore, a high degree of penetration through thick clouds at MW frequencies and higher sensitivity but less ability to penetrate clouds at IR and visible (VIS) frequencies. This makes MW, IR, and VIS observations ideal candidates for implementing a truly synergic approach. This complementarity has already led to fruitful synergies in various fields of meteorological science, as shown, for example, in [2], where the synergy of IR and VIS is exploited to estimate rainfall classes at a high spatial and temporal resolution, or in [3], where a combined MW-IR algorithm for convective precipitation estimation is described.

Scientific papers in satellite cloud retrieval using IR only, MW only or IR-MW combined data (source: Scopus)

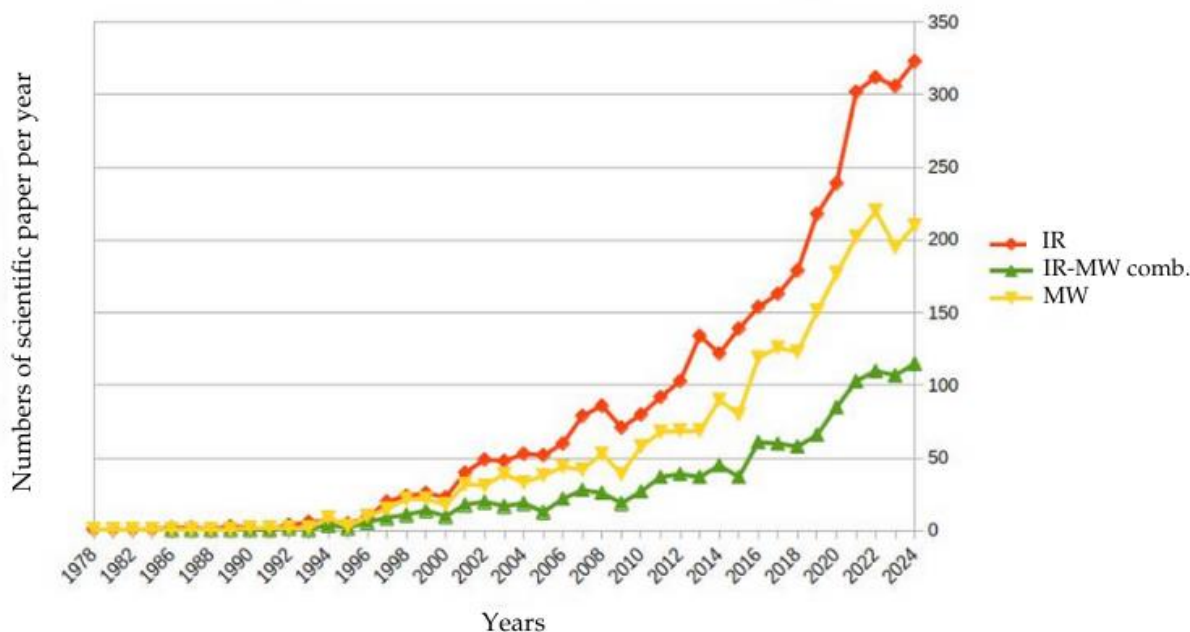


Figure 1. Number of scientific papers per year focusing on cloud parameter retrievals using only IR (red), only MW (yellow), or combined IR–MW (green) satellite passive observations (source: Scopus, <https://www.scopus.com/search/form.uri?display=advanced> (accessed on 27 November 2024)).

To gain insight into the benefits of a synergic approach and the challenges to be addressed, a deeper look at the current state of the art seems needed in order to also understand what has already been done in this direction and how studies have customized and adapted synergistic techniques to fit the remote sensing context. Thus, this work explores the most recent knowledge and development achieved in the field of targeted retrieval of cloud microphysical parameters, starting from observations performed in the VIS, IR, and MW wavelengths in either a stand-alone or complementary manner, with the aim of finding answers to the above-mentioned challenges. This review provides an overview of the techniques developed for retrieval with observations in each of the bands (MW and IR) individually, with their characteristics and main results. This work highlights the achieved improvements and discusses how some techniques have evolved, transformed, and merged to address specific challenges without going into the specific details of the individual strategies.

This paper is organized as follows: After a brief introduction to the key quantities considered for cloud microphysics research, the methods used to retrieve these cloud properties from IR-only and MW-only satellite observations are reviewed in Section 2. Section 3 is dedicated to methods developed to integrate MW and IR observations in order to improve the accuracy of cloud products, and Section 4 summarizes the main cloud parameter databases and retrieval methods. Section 5 discusses the main points and presents conclusions, highlighting the gaps and new challenges found during this review, and it finally suggests desirable future research work in this field.

2. Clouds Properties from Infrared and Microwave Satellite Observations

As already mentioned in the previous section, clouds influence many aspects of atmospheric physics, and their study can reveal a lot about meteorological phenomena and climate change. Clouds are essential to understanding the global hydrological cycle, assessing the Earth's radiation budgets, monitoring high-impact events, and forecasting the spatial and temporal distribution of precipitation. As for climatological aspects, clouds play a key role in the water cycle and the global energy balance, constituting one of the most complex protagonists of atmospheric physics and the climate machine. Clouds are, therefore, a very complex field of investigation, and each aspect constitutes a research field in itself with specific techniques and algorithms. For this reason, the study of clouds covers a very wide field, and there are many aspects related to clouds that are explored in depth, both from an operational point of view and from a more strictly scientific one, with the implementation of ad hoc techniques that allow for measuring the properties of interest. Among these, we mention methodologies for cloud detection and classification [4], precipitation estimation [5,6], and techniques for NWP assimilation [7,8]. For all these topics, we refer to the specific literature and the references therein. In this review, we limit our investigation to methodologies and algorithms for the study of the microphysical properties of clouds. These can be explored by exploiting some key quantities that can be retrieved from observations made via instruments operating in the MW, VIS, and IR spectra. Among the cloud microphysics characteristics, the main ones we refer to are the vertical profiles of cloud liquid water content (CLWC), cloud ice water content (CIWC) and their column-integrated values, the cloud liquid water path (CLWP), the cloud ice water path (CIWP), and, finally, the cloud drop and ice particle effective diameter (D_e ; in this review, we also refer to the effective radius, $D_e/2$).

2.1. Microwave Observations Only

Due to its long wavelength, microwave radiation can penetrate entire cloud layers and is particularly responsive to large particles; consequently, observations are more sensitive

to water vapor, clouds, and precipitation. Furthermore, given the different effects of liquid/ice water clouds on the measured brightness temperature (BT), the peculiarities of microwaves allow the detection of different types of clouds at different frequencies. For example, observations in the 23.8 and 89 GHz channels are more influenced by liquid than cirrus clouds. On the other hand, observations in frequencies close to the 157 and 183 GHz channels are more influenced by the presence of ice clouds. In the literature, several works exploit the knowledge acquired from MW radiometric applications consolidated since the late 1980s, which have seen the development of various methods to retrieve meteorological quantities based on physical and empirical methods.

The most used methods are reviewed below; they generally exploit different channels (23.8, 31.4, 90, and 183 GHz) to find information on cloud liquid water and atmospheric water vapor, and the 90 and 150 GHz and higher-frequency window channels to obtain information on ice clouds and the rain rate.

Early attempts to retrieve cloud microphysical parameters from MW radiance were mainly concerned with the knowledge of ocean surface winds [9], total precipitable water (TPW) [10], CIWP, CLWP and precipitation [11], and CLWP and cloud frequency [12] using the Special Sensor Microwave/Imager (SSM/I) measurements. Subsequently, various algorithms have been developed to meet the specifications of increasingly new sensors. This is, for example, the case for [13], where the development of a regression scheme to retrieve TPW and CLWP over the ocean using the channels at 23.8 and 31.4 GHz of the multichannel MW radiometer Advanced Microwave Sounding Unit (AMSU) is described. This algorithm, although based on the same TPW and CLWP retrieval theoretical background from the SSM/I, differs from the latter due to the geometric and spectral particularities of the two instruments. Several comprehensive comparisons between TPW and CLWP retrievals from AMSU and other satellite instruments (including SSM/I and Tropical Rainfall Measurement Mission Microwave Imager—TMI) or ground-based radiometers [14] can be found in the literature. Many works also demonstrate good agreement between AMSU TPW and radiosonde measurements, showing root mean square differences (RMSDs) of less than 3 kg/m² and biases of less than 1 kg/m² in the range between 5 and 60 kg/m². AMSU radiances have also been used for CLWP retrieval, for which it has been shown that AMSU time series and ground-based sensors follow each other in the range of 0–0.5 kg/m². As shown by [14], a comparison with other satellite measurements also yields good results despite a bias between AMSU and TMI for CLWP greater than 0.5 kg/m².

The measurements at the frequencies of 89 and 150 GHz of the microwave sounder AMSU were also used by [15] to formulate an algorithm for the retrieval of CIWP and D_e to exploit the ice particle scattering parameters. In the same work, a careful analysis of the main sources of error that can influence the retrieval process and a screening procedure to distinguish the scattering signatures between atmospheric clouds and surface materials were performed. It was shown that the recovered D_e is mainly influenced by two error terms, related to the particle bulk volume density (which, in this work, is assumed to be constant and equal to 600 kg/m³) and the cloud base (BT) estimate at 89 and 150 GHz. Overall, these two terms impact the D_e value by 10% (considering a 3% error in the BT temperature) and between 5% and 20% (considering a 30% uncertainty in the bulk volume density of the particles). A similar analysis was conducted for the retrieved values of CIWP, noting that they are affected not only by uncertainties in the estimation of the BT and particle volume density but also by the retrieved D_e itself. The authors estimated that a 30% error in the bulk volume alone would result in a 25% error in the retrieved CIWP. Unfortunately, due to the lack of sensitivity at 89 GHz, this procedure seems to fail to detect thin cirrus clouds surrounding precipitating areas. In these cases, using even higher frequencies or measurements in the IR/VIS region may be effective.

Again in reference to the AMSU radiometer, ref. [16] describes the application of the algorithms in [13] for cloud and precipitation products and present a methodology to examine the instrument performance after launch. In this work, the 23.8 and 31.4 GHz AMSU channels are exploited to retrieve cloud liquid water and total precipitable water. In this case, the results obtained via the algorithm are significantly improved by using global analyses of surface wind and sea surface temperature from the NWP model. In a similar way, the 89 GHz and 150 GHz channels are used to estimate the ice water path associated with thick ice clouds. However, following this routine method, the uncertainty in the retrieval of cloud ice water path and particle size remains high due to an unknown particle bulk volume density.

Starting from the past experience with SSM/I and, subsequently, with the hydrological products obtained from the operational algorithms based on the AMSU sensor series, ref. [17] describes the operational Microwave Surface and Precipitation Products System (MSPPS) product system, which represents an upgrade to the previous ones and provides near real-time (only a few minutes of processing) hydrological products from AMSU. In their paper, ref. [17] outline the retrieval algorithms' status as of September 2004 and present several comparisons with ground-based measurements and other satellite products. In detail, CLWP and TPW are estimated using 50 and 23.31 GHz channels, primarily based on the algorithms reported in [16], while the algorithm in [15] is used to simultaneously derive CIWP and ice particle effective diameter D_e from 89 and 150 GHz. The formulas for computing the TPW and CLWP use coefficients valid only for the sea surface, unlike the calculation of CIWP, which is valid on both land and ocean with the background surface free of ice/snow, as it is inferred from AMSU lower-frequency channels. Comparisons between the AMSU-derived TPW and both the radiosonde-derived TPW for nine stations and the radiometer-derived TPW for ARM sites representative of open ocean conditions on Manus Island and Nauru are shown. A similar approach is applied to AMSU-derived CLWP with respect to the ARM-derived CLWP. It is worth noting that, due to the poor spatial homogeneity of the CLWP compared to the TPW, the former requires special treatment to better use it for the validation of AMSU data, as described by [13]. As a result, a correlation of about 0.6, an RMSD of about 0.05 kg/m^2 , and a small bias of less than 0.01 kg/m^2 was found for approximately 190 and 160 CLWP match-up points in the case of NOAA-15 and NOAA-16, respectively. To reduce the non-uniformity of the data distribution in the available range, a further analysis was conducted by binning CLWP retrievals into 0.01 kg/m^2 bins using the ground-based ARM data. The binned analysis leads to the following main conclusions: (i) there is very little bias in the AMSU-derived CLWP for values $> 0.3 \text{ kg/m}^2$, validating the reliability of CLWP retrieval from 31.4 GHz observations under non-precipitation conditions; and (ii) there is some angular dependency on the retrievals, most likely attributed to the larger FOV (for this and other abbreviations in the text, please see the List of Abbreviations and Acronyms at the end of the document) of the AMSU-A sensor as the view angle increases. CLWP derived from AMSU on NOAA-16 and CLWP generated from the Advanced Microwave Scanning Radiometer for EOS (AMSR-E) were also compared, and good qualitative agreement but significant divergences were found from a quantitative point of view, presumably due to a difference in the acquisition spectral channels of the two instruments. Overall, global mean differences of the order of 10% with spatial correlations on the order of 0.75 were found. Following the same methodology, they also concluded that the CLWP affects the agreement of AMSU TPW retrievals with radiosondes, with larger biases than relatively higher CLWP values. Analogously, the TPW RMSD also increases, ranging from about 10% for $\text{CLWP} < 0.2 \text{ kg/m}^2$ to over 15% for $\text{CLWP} > 0.8 \text{ kg/m}^2$.

In the work of [18], the described estimation of the vertical distribution of liquid water and its integrated amount on a water surface is the first step of a microwave geophysical retrieval algorithm based on the application of a forward radiative transfer model within the combined sounding suite exploiting the Atmospheric Infrared Sounder/AMSU-A/Humidity Sounder for Brazil (AIRS/AMSU/HSB). The methodology implemented for CLWC retrieval is based on a moisture condensation model that uses the relative humidity retrieval for cloud formation, which makes the retrieval process more robust than usual techniques because it is less sensitive to retrieved temperature profile errors and to the humidity field within instrument footprint horizontal inhomogeneities. The results are validated via comparisons with ground-based radiometric measurements with reference to the retrieved CLWC and with relative humidity profiles from radio-sounding launches dedicated during the Aqua satellite overpass with respect to the vertical distribution (mean cloud pressure). The estimation of cloud liquid profiles and the integrated amount over a water surface using the AMSU/HSB algorithm seems to offer some reliability. However, it would be necessary to expand the comparison dataset with a wider range of cloud heights and to incorporate infrared measurements into the process. Unfortunately, a careful characterization of the cases in which the algorithm does not provide the expected results is missing from this work.

An accurate and computationally not very expensive approach to atmospheric profile retrieval is proposed by [19]. The purpose of their effort is to develop an iterative technique based on the one-dimensional variational method (1D-Var) to simultaneously retrieve water vapor and temperature profiles, as well as cloud water profiles. This purpose is reached by combining both the AMSU window and sounding channels using a synergic method. The 1D-Var microwave principal module for retrieval is developed in sequential key steps; first, it computes water vapor, temperature, and cloud liquid water profiles using only AMSU-A data at frequencies less than 60 GHz. Then, rain and ice water are derived using AMSU-B data at 89 and 150 GHz. Ultimately, temperature and water vapor profiles are more refined by means of all AMSU-A/B sounding channels (50–60 and 183 GHz), while the profiles of cloud, rain, and ice water contents are forced to those earlier derived. Validation work was conducted on the 1D-var retrieval algorithm in terms of water contents. A comparison with radiosonde data and collocated satellite measurements showed a relatively small bias (less than 0.3 kg/m²) and RMSDs of 2.7, 2.3, and 2.5 kg/m², evaluated against data on different NOAA platforms (NOAA-15, -16, and -17, correspondingly). Comparisons were also made over sea and land (but ignoring the data over high latitudes beyond 60° north and south) between the AMSU-derived TPW and the GFS data assimilation system (GDAS). In this case, the bias and RMSD values of the zonal means are 0.15 and 0.75 kg/m², respectively.

Applications of the one-dimensional variational method to the problem of retrieving the hydrological properties of the troposphere are also found in [20–22]. In these works, the authors present a mini-satellite constellation design, implementing millimeter-wave (MMW) scanning radiometers. The proposed mission objective is to retrieve the troposphere thermal and hydrological properties, in particular temperature and water vapor profiles, rain rates, and snowfall rates. The channels are selected following a ranking based on a reduced entropy method between 90 and 230 GHz. The authors point out that the mission was restricted to the feasibility study, so only simulated data are available. In particular, in [20], the benefit of a 1D-Var scheme for deriving hydrometeor profiles from the proposed set of MMW observations is quantitatively evaluated, and the results are shown for the channel combination that achieved the best performance in the reduced entropy ranking (10 channels from 89 to 229 GHz). Furthermore, the algorithm performance in terms of the residual error between the measured profiles and the profiles retrieved from simulated data using 1D-Var was examined, showing good agreement for the hydrometeor profiles

retrieved over land and sea and for a summer/winter season at different latitudes. The standard error statistics show a rather small contribution to the forecast, more significant over the sea than over land, for both liquid and ice cloud content. The four selected configurations of MMW radiometers' overall accuracy were evaluated by [21], exploiting two statistical inversion schemes, multiple regression and maximum likelihood. The performances of the two schemes were similar, showing only slightly algorithm-dependent retrieval uncertainty.

Using multiple regression with their best channel configuration (10 channels), the authors report the following correlation coefficient (R), root mean square (RMS), and uncertainty (σ):

- CLWP (0–1.4 kg/m²): R = 0.70; σ = 0.08 kg/m² over land; R = 0.87; σ = 0.04 kg/m² over the ocean.
- CIWP (0–0.25 kg/m²): R = 0.58; σ = 0.01 kg/m² over land; R = 0.64; σ = 0.03 kg/m² over the ocean.

The correlation increased considerably for rain-sized ice particles (i.e., graupel), R = 0.97 over the ocean and 0.97 over land.

In these works, it is also shown that the CLWC profiles' expected RMS uncertainty is within 0.1 g/m³ over land and 0.04 g/m³ over the ocean; however the authors warn that these results should be valid for the available dataset only. Overall, they report lower performances for non-precipitating CLWC and CIWC profiles than for precipitating liquid (rain) and ice (graupel) profiles, over both land and ocean.

A further impetus to the knowledge of cloud microphysical properties is provided through the development of innovative processing techniques and advances in analytical and computational capabilities. In recent years, the expanding field of artificial intelligence has promised to provide a new opportunity for making cloud microphysical products increasingly accurate and opening the way to a new understanding in this field.

An example of the application can be found in [23], where the retrieval of TPW and CLWP from SSM/I and AMSR-E is addressed with a neural network (NN) algorithm. This approach, which can be applied to high-latitude open water areas, has been shown to be a better choice than the conventional regression techniques (validation against radiosonde data from a polar station). The validation process shows that the resulting RMSD for the retrieval products is 1.09 kg/m² for SSM/I and 0.90 kg/m² for AMSR-E, respectively. Moreover, only for SSM/I, the TPW algorithm is compared with the global operational algorithm described in [24], showing retrieval errors of 1.34 kg/m² and 1.90 kg/m² (about 40% worse) and demonstrating the advantages of the NN approach of [23].

Radiative transfer models can also be used to improve the quality of retrievals. For example, in the case described by [25], the retrieval of CIWP and the effective ice particle diameter, D_e , from SSMI/S are based on a simplified two-flux radiative transfer model applied as a three-parameter equation model. The advantage of this procedure is that, due to the conical scan geometry of Special Sensor Microwave Imager/Sounder (SSMIS/S), the retrieved CIWP is less dependent on the scan position. Furthermore, several important sources of errors that may affect the quality of retrievals are identified and analyzed. In particular, the authors identify the error in the cloud base temperature estimate and the effective particle diameter as the main sources of uncertainty in the CIWP retrieval, as their overestimation could lead to the underestimation of the CIWP for the smallest particles.

In [26], the Microwave Integrated Retrieval System (MIRS) algorithm, a 1D-Var scheme developed at NOAA since 2007, is applied to data from the Advanced Technology Microwave Sounder (ATMS) onboard the Suomi National Polar-Orbiting Partnership (SNPP) satellite. The approach followed is a simultaneous inversion obtained by coupling the land–ocean–atmosphere–cryosphere process to ensure that all radiances are fitted simul-

taneously and that geophysical reliability is also satisfied. The performance of the MIRS was evaluated using both in situ measurements (radar, radiosondes, gauges, and surface sensors) and analyses from the European Centre for Medium-Range Weather Forecasts (ECMWF) and heritage algorithms (e.g., MSPPS). In fact, MIRS is expected to replace MSPPS as the NOAA operational product through a gradual, multi-phase transition. The results in [26] show a correlation of 0.99 and an RMSD of 3.1 kg/m^2 for a one-day validation of TPW against ECMWF. This daily validation is carried out operationally at “<https://www.star.nesdis.noaa.gov/mirs/geonwp.php> (accessed on 18 January 2025)”. However, the authors are aware of the difficulty of directly evaluating the hydrometeor parameters due to the nonexistence of consistent ground truth, and therefore, given the algorithm implemented in MIRS, they assume that the validation of the rain rate is a proxy for the validation of all MIRS-based hydrometeors. Following this approach, the expected values for bias and rms uncertainty are 1.5 and 2.5 kg/m^2 over land and 1.7 and 2.2 kg/m^2 over the ocean in the case of TPW, and 0.03 and 0.10 kg/m^2 over the ocean in the case of CLWP.

Ref. [27] proposes two algorithms to estimate TPW and CLWP over oceans by assimilating microwave observations from sensors on board the FY-3D satellite. Both algorithms combine two oxygen channels (52.80 and $118.75 \pm 2.5 \text{ GHz}$) to address the lack of low-frequency window channels’ (23.8 and 31.4 GHz) FY-3 sensor. A performance analysis of the two algorithms was conducted using four groups of experiments and comparing the results from FY-3C double oxygen absorption bandwidth with the retrievals using the classical method of [13] applied to MetOp-B AMSU observations at 23.8 and 31.4 GHz . The CLWP retrievals from the double oxygen band show correlation coefficients, bias, and rms in agreement with those obtained through the traditional AMSU scheme. On the contrary, the performance of TPW retrievals is significantly worse than the retrievals with the traditional AMSU scheme.

Still with reference to FY-3C and strategies to overcome the lack of observations in the two low-frequency channels, ref. [28] describe a technique based on machine learning to generate BT at the two missing low-frequency channels from higher-frequency observations with mean absolute errors between 3 and 4 K. The statistical inversion method used to retrieve TPW and CLW over oceans also compares well in magnitude and distribution with Suomi NPP ATMS estimates.

The article by [29] presents an assessment of the performance of MIRS CLWP retrievals. The CLWP product is validated against both ground radiometric measurements (ARM site in Azores, Portugal) and a satellite reference dataset (NASA GPROF). In this work, the collocation method for the ground-based comparisons considers observations within 30 min from the satellite overpass and an FOV within a 3 km radius centered on the site. The dataset includes data collected over 3 years (for a total of 1535 match-ups), and the results show an overall all-season correlation coefficient, bias, and standard deviation of 0.59, -0.065 kg/m^2 , and 0.2 kg/m^2 , respectively. In detail, the seasonal analysis shows good correlation coefficients (greater than 0.5 for all seasons), with a maximum value for autumn (0.66) and a minimum for summer (0.51). Similarly, as regards the bias, the values are between -0.052 kg/m^2 (found in autumn) and -0.076 kg/m^2 (found in summer). Finally, the comparison with GPROF shows a correlation coefficient, bias, and standard deviation equal to 0.71, 0.005 kg/m^2 , and 0.07 kg/m^2 , respectively.

Ref. [30] uses a neural network approach to retrieve the snow ice water path, liquid-water path, and integrated water vapor from millimeter and submillimeter brightness temperatures from airborne radiometers (ISMAR and MARSS). The database for training neural networks was built with ICON-NWP atmospheric profiles and Atmospheric Radiative Transfer Simulator (ARTS) simulations. Comparing the retrieved integrated water

vapor (IWV) values with those measured via the 12 dropsondes reveals a mean difference between them of 0.5 kg/m² and an RMSD of 0.8 kg/m².

Recently, the progress of technology, combined with the advancement of MW radiometry, has allowed the use of cm-sized mini-satellites (cubesat) for Earth observation. Time-Resolved Observations of Precipitation Structure and Storm Intensity with a Constellation of Smallsats (TROPICS) and the Temporal Experiment for Storms and Tropical Systems Technology-Demonstration (TEMPEST-D) are two NASA-funded missions that exploit MW radiometers on board the cubesat modules. The aim of TROPICS [31] is to provide profiles of water vapor and temperature, as well as the liquid/ice rain rate, utilizing seven channels near the oxygen absorption line at 118.75 GHz, three channels near the line of the water vapor absorption at 183 GHz, and single channels near 90 and 205 GHz. TEMPEST-D [32] aims to provide measurements of water vapor profiles, CLWP, and CIWP with an accuracy of 0.1 kg/m², exploiting frequencies between 89 and 183 GHz. Note that some of these channels (e.g., the 118 GHz band and the 205 GHz channel) have never been tested in space and could serve as proxies for channels foreseen for the MicroWave Imager (MWI), 118.75 GHz, and MicroWave Sounder (MWS), 229 GHz. The TEMPEST-D measurements appear to be of similar quality to the MHS measurements, as highlighted in [33], both for the consistency between the TEMPEST-D and the Microwave Humidity Sounder (MHS) brightness temperatures and for that of the atmospheric parameters retrieved from TEMPEST-D via the Colorado State University (CSU) 1D-VAR algorithm with those retrieved from MHS. This applies to both MIRS retrievals and CSU 1D-VAR retrievals.

Table 1 summarizes the main information for each study reviewed in Section 2.1, the sensors and channels used, and the products investigated.

Table 1. Microwave observations-only recap table.

Authors	Year	Satellite		Main Features	Uncertainty or Accuracy of the Method (When Declared/Applicable)
		Sensor	Channel Frequency [GHz]		
Goodberlet et al. [9]	1989	SSM/I	-	Retrieval includes ocean surface wind	ACC = ± 2 m/s
Alishouse et al. [10]	1990	SSM/I	-	CLWC	RMSD% = 30%
Bauer and Schluessel [11]	1993	SSM/I	-	CLWP, CIWP, TPW, RR	RMSD _{WV} < 0.78 g/cm ²
Han and Westwater [14]	1995	SSM/I, AMSU, TMI	-	Several retrieval comparisons	-
Weng et al. [12]	1997	SSM/I	-	CLWP, cloud frequency	-
Wentz and Spencer [24]	1998	SSM/I	-	TPW	RMSD _{WV} = 5 mm
Grody et al. [13]	2001	AMSU	23.8, 31.4	TPW, CLWP over ocean	RMSD _{TPW} < 3 mm
Zhao and Weng [15]	2002	AMSU	89, 150	CIWP, D _e , CB	5% < RMSE _{D_e,%} < 20%

Table 1. Cont.

Authors	Year	Satellite		Main Features	Uncertainty or Accuracy of the Method (When Declared/Applicable)
		Sensor	Channel Frequency [GHz]		
Weng et al. [16]	2003	AMSU	23.8, 31.4	Evolution of [13] G by using SST and SW from NWP models	-
Ferraro et al. [17]	2005	AMSU	-	MSPPS	-
Liu and Weng [19]	2005	AMSU-A/B	50–60, 89, 150, 183	1D-Var retrieval algorithm	RMSE _{TPW} = 2.5 mm
Rosenkranz [18]	2006	AIRS, AMSU, HSB	-	CLWC profiles	-
Marzano et al. [20]	2009	MMW	-	-	-
Marzano et al. [22]	2010	scanning radiometers	89–229	CLWC, CIWC profiles	-
Marzano and Cimini [21]	2010	-	-	-	-
Bobilev et al. [23]	2010	SSM/I, AMSR-E	-	TPW, CLWP	RSME _{VW} = 1.34 kg/m ²
Sun and Weng [25]	2012	SSM/I/S	-	CIWP, D _e	-
Boukabara et al. [26]	2013	ATMS	-	NOAA MIRS algorithm outputs	13% < SD _% < 24%
Dong et al. [27]	2017	FY-3D	52.8, 118.75 ± 2.5	TPW, CLWP	RMSE _{TPW} = 3.19 kg/m ²
Liu et al. [29]	2018	ATMS	-	CLWP	SD _{CLWP} = 0.2 mm
Brath et al. [30]	2018	ISMAR, MARSS	-	SIWP, LWP, IWV	MFE _{IWV,low} = 2 kg/m ²
Blackwell et al. [31]	2018	TROPICS	90, 118.75, 183, 205	WV profiles, LP, IP	-
Reising et al. [32]	2018	TEMPEST-D	89–183	WV profiles, CLWP, CIWP	-
Han et al. [28]	2021	FY-3D	52.8, 118.75 ± 2.5	TPW, CLWP	-

2.2. Infrared Observations Only

Passive IR observations are mainly sensitive to atmospheric humidity, temperature, liquid/ice clouds, and trace gases. Approaches to deriving cloud properties from infrared observations were among the first methods developed in the satellite meteorology initial years [34–36], while aspects of cloud microphysics, such as cloud optical thickness and particle size [37–39], were developed later.

Inferring very good values for cloud optical thickness and the effective radius is the aim of the statistical technique developed by [40], a new discrete ordinates radiative transfer method, and asymptotic terms for thick layers reflection function were developed. A non-absorbing visible wavelength (0.75 μm) and two absorbing wavelengths (2.16 and 3.7 μm) are used for the effective radius and optical thickness of stratiform cloud retrievals. To reduce ambiguity in deriving the effective radius for optically thin clouds, the two absorbing near-infrared wavelengths are used. However, for optically thin clouds, the retrievals become uncertain. Following [41], the optical thickness and the effective radius uncertainty (5%) are analyzed as a function of errors in the measured reflection function, as well as in the phase function surface albedo. Finally, their method's performance using Advanced

Very-High-Resolution Radiometer (AVHRR) observations over the ocean (channels at 0.64, 3.75, and 11.0 μm) was studied by [42], finding good agreement between satellite and in situ products. The cloud retrieval schemes described in [40,42] have also been widely adopted in the simultaneous estimation of cloud optical thickness and effective cloud particle radius and in the generation of operational JAXA and NASA satellite products [43,44].

Another method based on a radiative transfer model to retrieve the radii of cloud particles in liquid-water clouds using AVHRR data is described in [45]. This method shows significant seasonal and diurnal variations in the effective radii of droplets, particularly at lower latitudes.

An approach based on AVHRR observations at 0.63 and 1.6 μm for CLWP retrievals is reported by [46]. A cloud analysis through the phase classification of cloud particles and estimation of optical thickness and effective radius is described. The validation of the retrieved CLWP is carried out against ground-based observations retrieved from microwave radiometers during the campaigns of the Cloud Liquid Water Network project (CLIWA-NET). It is important to remember that many aspects of atmospheric conditions (such as, for example, the wind speed at cloud height and the structure of the cloud field) influence the relationship between satellite observations and ground-based measurements, causing a spatial and temporal discrepancy between the two observing strategies. On average, CLWP derived from satellite and ground observations correlates with a 0.88 correlation coefficient with the slope of the linear regression close to 1 and the intercept smaller than 10 gm^2 . No systematic bias was found even though the CLWP from a satellite is generally higher than that measured through a ground-based approach. The authors conclude that this is an effect of the satellite effective radius, used to link optical thickness to CLWP, which is representative of larger particles at the cloud-top. This may cause a CLWP overestimation because of the particle-size overestimation [47].

Refs. [48,49] propose to partially solve this problem by making the parameterization of the vertical droplet size distribution in radiative transfer calculations more realistic. Ref. [50] shows that airborne multispectral Moderate Resolution Imaging Spectroradiometer (MODIS) Airborne Simulator (MAS) data over the Arctic with the 1.62 μm and 2.13 μm algorithm make the determination of the effective radius and the optical thickness of water clouds more reliable over snow and sea ice surfaces. The explanation for this behavior lies in the very low surface reflectance of snow and sea ice at these wavelengths. For these reasons, the reflectance contrast of the liquid-water clouds compared to the underlying dark surface is relatively strong. However, this algorithm is less reliable due to the ice particles' strong absorption in both bands for ice clouds.

Based on the work of [42], ref. [51] used cloud-reflected solar radiances for both visible and near-infrared wavelengths to develop a retrieval algorithm capable of analyzing cloud microphysical parameters on a global scale, with good agreement between the results and in situ measurements.

The work of [52] falls under the framework of the European Organisation for the Exploitation of Meteorological Satellites (EUMETSAT) Satellite Application Facility on Climate Monitoring (CM SAF) and reports a comparison between the Meteosat Second Generation-Spinning Enhanced Visible and Infrared Imager (MSG-SEVIRI) and AVHRR cloud optical thickness and cloud liquid path retrievals derived from the Cloud Physical Properties (CPP) scheme. The retrieval of the physical properties of clouds is based on the principle that the clouds' reflectance at a non-absorbing wavelength in the visible region (0.6 or 0.8 μm) is strongly related to the optical thickness, while it does not depend on the particle size. In contrast, the clouds' reflectance at an absorbing wavelength (1.6 or 3.8 μm) is mainly related to the particle size. Consequently, using operational calibrations, SEVIRI and AVHRR cloud properties differ significantly; this recalibration improved the

differences between the cloud properties retrieved via SEVIRI and AVHRR, bringing the values below 5%.

Ref. [53] addresses the problem of retrieval of cloud properties (effective radius, optical thickness, and cloud temperature) from MODIS infrared imagery using an NN approach. The multilayer perceptron (MLP) architecture was trained with supervised backpropagation with a momentum algorithm. To evaluate the robustness of the method, several sources of uncertainties were analyzed, such as the measured radiance, cloud temperature specifications, and lower boundary conditions. The total error lies between 0.25 and 0.45 μm for the effective radius and between 0.05 and 0.88 for the COT when simultaneous uncertainties are considered. According to the authors, these uncertainties dominate the uncertainty budget over the errors introduced via the NN inversion, estimated within 1%.

Ref. [54] presents the Integrated Cloud Analysis System (ICAS) algorithm for retrieving the macroscopic, physical, and optical properties of clouds. ICAS was developed based on the optimal estimation approach, and it exploits MODIS observations in Thermal InfraRed (TIR) bands. Four TIR bands centered at 8.6, 10.4, 11.2, and 12.4 μm are identified in the atmospheric window to retrieve parameters such as cloud-top height (CTH), COT, and the effective radius, $D_e/2$, which are sensitive to the properties of clouds. Performance is tested using retrieval simulations, showing that ice cloud properties are inferred with high accuracy for COT between 0.1 and 10. Cloud-top pressure is retrieved with an uncertainty of less than 10% when COT is greater than 0.3. ICAS is also applied to the multiband observations of the Himawari-8 instrument [55]. A sensitivity study is performed to demonstrate that the addition of the single CO_2 band of Himawari-8 is effective for CTH estimation. For validation purposes, a systematic comparison is conducted between the retrieved cloud properties and collocated active remote sensing counterparts with small time delays. Reasonable agreement is found for single-layer clouds, while multilayer cloud systems with optically thin upper clouds overlapping lower clouds are the main source of error. The variance in measurement model differences within an area of $(10 \text{ km})^2$ is used to estimate measurement noise. Comparisons are performed between ICAS-derived data and the raDAR/liDAR (DARDAR) cloud product to validate the retrievals. The DARDAR project provides cloud mask vertical profiles and ice cloud properties, including the ice water content, D_e , and extinction coefficient obtained from combined MODIS observations, CloudSat radar, and Cloud-Aerosol Lidar and Infrared Pathfinder Satellite Observation (CALIPSO) lidar, as well as TIR measurements, with a vertical resolution of 60 m and a horizontal spatial resolution of 1.1 km.

Data from high-spectral-resolution infrared sounders can provide consistent micro-physical cloud properties, and the benefits of their use have been recognized since the 1970s [56]. Subsequently, applications to cloud properties were explored for data from both aircraft (e.g., [57,58]) and satellites (e.g., [59,60]).

A technique for inferring the microphysical and radiative properties of water and cirrus clouds is presented in [57]. This technique, validated using theoretical calculations, is applied to ground-based and NASA aircraft-based Hyperspectral Imaging Sensor (HIS) instrument observations, along with cloud lidar backscatter and in situ atmospheric temperature and humidity observations. This study describes the cloud optical properties' spectral variability within the window region.

A method for deducing semitransparent ice Clouds Optical Thickness (COT < 5) using AIRS measurements is presented in [60]. In this work, the sensitivity of AIRS spectral BT and Brightness Temperature Differences (BTD) values between wavenumber pairs for COT is studied. The spectral BTs within the 1070–1135 cm^{-1} region (atmospheric window channels) are sensitive to the ice COT and similarly for the BTD between 900.562 cm^{-1} (at-

atmospheric window) and 1558.692 cm^{-1} (strong water vapor absorption band). Analogously, the BTD is sensitive to ice COT between the channels 1587.495 cm^{-1} and 1558.692 cm^{-1} , respectively, a moderate and a strong water absorption channel. The method performance is evaluated by comparing the ice COT obtained from the AIRS observations with those estimated from MODIS (1.38 and $0.645\text{ }\mu\text{m}$ bands), suitably collocated and degraded to the AIRS spatial resolution. There is substantial agreement regarding the COT for thin to moderately thick cirrus clouds ($\text{COT} < 5$). Instead, as COT increases, the COT retrieved via AIRS tends to be lower than MODIS. This may be due to the saturation of the BTD signal for large COT values.

The methodology described in [60] and based on two or more channels in the IR window is sometimes known as the “split-window method”. In the literature, there are many applications of this approach, which, although applicable to all clouds, is more powerful in the case of high semitransparent ice clouds [61]. Some applications can be found, for example, in [62] (for the retrieval of microphysical properties of semitransparent cirrus clouds using $11\text{ }\mu\text{m}$ and $12\text{ }\mu\text{m}$ AVHRR data) and in [61] (to explore its usefulness for the generation of a multidecadal climatology based on AVHRR data of cloud temperature, emissivity, and a microphysical parameter). Split-window ($11\text{--}12\text{ }\mu\text{m}$) brightness temperature differences are used by [63] to identify the cloud type, while the high sensitivity to the predominance of small ice crystals of the BT difference between two bands in the atmospheric IR window is exploited by [64] to develop a technique for the unambiguous identification of thin cirrus clouds with effective radii smaller than $20\text{ }\mu\text{m}$. Split-window MODIS channels are also applied by [65] for the retrieval of the liquid-water fraction from cold clouds in the case where the liquid fraction is less than 50% of the total condensate.

The theoretical basis for estimating the ice cloud microphysical properties fusing high-spectral-resolution infrared observations was reviewed by [66]. From the simulations developed in their work, it is possible to see how the slope of the IR BT spectrum between 790 and 960 cm^{-1} is sensitive to the effective particle size; furthermore, the infrared brightness temperature appears to be highly sensitive to optical cloud thickness in the $1050\text{--}1250\text{ cm}^{-1}$ region. From these spectral features’ examination, the authors illustrate a method to simultaneously retrieve the visible optical thickness and effective ice cloud particle size from high spectral resolution infrared data. From the uncertainty analysis, it is concluded that the retrieved COT and effective particle size uncertainties have a small range of variation. Regarding the uncertainty of the particle size, a value lower than 15% is found in the case of a cloud temperature uncertainty of 5 K or a surface temperature uncertainty of 2.5 K. However, concerning the optical thickness, the corresponding uncertainty value is between 5% and 20%, depending on the COT value.

Ref. [67] studies the advantages of a combined approach using the MODIS and AIRS products to obtain the microphysical properties of clouds during both day and night. MODIS can provide mask products (cloud mask, cloud phase detection, and cloud classification) and cloud microphysical products, while AIRS radiance measurements are useful for retrieving the COT and particle size of clouds. In detail, the cloudy condition (clear/cloudy, ice/water, and single/multilayer) of the AIRS subpixel is characterized by the MODIS cloud mask with a spatial resolution of 1 km during both day and night. Subsequently, with the operational MODIS COT and cloud particle size as the background information, 1D-VAR can be used to retrieve the microphysical properties of clouds during the day, while minimum residual (MR) is used both during the day and during the night. In both approaches (1D-VAR and MR), the Cloud-Top Pressure (CTP) is derived from the radiances acquired via AIRS at CO_2 channels, while the cloud phase is inferred from the collocated MODIS 1-km phase mask. The authors compared 1D-VAR results with the operational MODIS products and MR cloud microphysical property retrievals for a case study and

reported that 1D-VAR retrievals have a great correlation with both the operative MODIS cloud products and MR cloud retrievals.

Ref. [68] presents a physical inversion scheme for clear/cloudy radiance observed with ultra-spectral infrared sounders to simultaneously retrieve atmospheric thermodynamic, surface parameters and cloud microphysical parameters. To improve an iterative background state defined by an eigenvector regression retrieval, a 1D-VAR approach is used. Cloud-top height can be estimated with quite high accuracy (the error is less than 1 km), for both optically thick and thin clouds. Finally, it is highlighted that using a more realistic ice-cloud habit could improve the retrieval performances.

The paper by [69] aims to use all available Infrared Atmospheric Sounding Interferometer (IASI) channels for the simultaneous retrieval of atmospheric temperature, humidity, and cloud properties by applying an Empirical Orthogonal Function (EOF) transformation to convert IASI channel radiance spectra into super-channels. Since it is shown that approximately 100 super-channels are sufficient to capture the information content of all the spectra, the calculation of both super-channel magnitudes and derivatives with respect to the atmospheric profiles and other properties can be performed via a Principal Component-based Radiative Transfer Model (PCRTM). This super-channel retrieval algorithm is applied to the IASI spectra acquired during the Joint Airborne IASI Validation Experiment (JAIVEx) field campaign.

Ref. [70] also refers to the IASI spectrometer, describing the operational IASI L2 processing chain (version 5) structure and counting the single retrieval modules, their algorithms, and a summary of different performance evaluation validation studies. A wide range of satellite products (including the Cloud-Aerosol Lidar with Orthogonal Polarization (CALIOP), the Advanced Along-Track Scanning Radiometer (AATSR), MODIS, AVHRR, and SEVIRI), numerical weather prediction, chemistry models, and in situ measurements (including radiosondes and buoys) are used to validate the retrieved geophysical parameters. The cloud detection, cloud cover, height, and phase included in L2 products are also evaluated. In detail, to assess cloud detection, an NN test is also added to the tests based on NWP and AVHRR, which increases the overall cloud detection capacity by roughly 25% compared to the NWP test alone, allowing the achievement of an overall success rate of over 90%. The different spectral emissivity that characterizes water and ice clouds in the spectral region between 8 and 12 μm allows the retrieval of the cloud phase. Ice clouds are identified through an additional test, applicable only in version 5, which takes advantage of the fact that super-cooled water cannot exist at temperatures below $-40\text{ }^{\circ}\text{C}$. The validation of the cloud phase detection process was performed using a co-located and globally distributed IASI and AVHRR dataset. The results confirm a good performance of the tuned algorithm which, in its final version, correctly detects 84.5% of the cloud phases, 97.3% of the ice samples, and 84.6% of the liquid samples. Worse performance is obtained for the detection of mixed-phase clouds; only 5.5% of this type is correctly identified, as most of these are detected as ice clouds. CTP is retrieved with a bias between 30 hPa bias and 50 hPa std compared to ground-based radars. The correlation coefficients with satellite lidar observations from CALIOP are 0.9. Furthermore, for the IASI CTP, the validation shows a bias of 15 hPa between 1000 and 550 hPa and std ≈ 90 hPa. Above 550 hPa, the dispersion is less (std ≈ 60 hPa), although the bias is greater.

In preparation for the direct assimilation of CLWC and CIWC profiles into 3D-Var, ref. [71] reports the evaluation of the feasibility of adding such profiles into the control vector of a 1D-Var assimilation system. This approach avoids the usual use of cloud parameters (effective cloud fraction and CTP), typically inferred from a CO_2 slicing algorithm, and cloud modeling using single-layer clouds [36]. CLWC, CIWC, and cloud fraction profiles are included via the RTTOVCLD interface of Radiative Transfer for TOVS (RTTOV) 10.1

(see [72], Section 2.6.1). RTTOVCLD allows multilayer mixed-phase clouds (two types of clouds per layer). Results from the simulation experiments (OSSE) demonstrate that 1D-Var works reasonably, adding an ice or liquid-water cloud in the correct region of the atmosphere. Furthermore, this study, which is limited to homogeneous cloud scenes with small background offsets, demonstrates that CIWC information is obtained for high opaque clouds, whereas little information is extracted for CLWC.

Using the identical 1D-Var framework, ref. [73] exploited a reduced number of IASI channels for data assimilation in cloudy sky. Following the approach in [74], information loss can be minimized through channel selection. This paper demonstrated that the channel selections are practically independent of the air-mass type and can improve the cloud variables' retrieval by 8% rms compared to the operational dataset exploited at NWP centers.

In a follow-up study, ref. [75] observed a meaningful reduction in the forecast error, particularly for CIWC, but also for CLWC. On average, a CIWC error reduction of 15–20% is achieved for semitransparent clouds versus 9% for opaque clouds, compared to 10% for the CLWC of semitransparent clouds and 3% for opaque clouds. This is not surprising, as the CLWC is known to be not well analyzed through 1D-Var, probably due to the relatively small sensitivity of the IR data to liquid cloud. In any case, the persistence of cloud information produced via a 1D-Var assimilation of cloudy IASI radiances into a convective scale NWP is established. The authors suggest that CLWC analysis could be better constrained using MW radiances.

Unlike the previous approaches, ref. [76] retrieve geophysical properties from the single FOV spectral radiances acquired via IASI under any conditions, using a PCRTM-based physical inversion approach. In their study, they show the excellent performance of the PCRTM retrieval method in detecting thin clouds with a COT as low as 0.04, revealing the extreme sensitivity of the developed algorithm to ultra-thin clouds. However, worse results are found for $COT > 4$.

A different approach is used in the work of [77], where cloud property retrieval through the use of the Clouds from Infrared Sounders, developed at LMD (CIRS-LMD), is described. In this case, the channels around the 15 μm CO_2 absorption band are considered. These channels can provide the highest cloud layer in the case of multilayer clouds, as well as the pressure and emissivity of the clouds in the case of a single cloud layer. This scheme has been applied to AIRS and validated with CALIOP's high-resolution cloud vertical profiles, showing satisfactory results regarding the retrieved cloud height, which corresponds well to the maximum backscatter measured via CALIOP for both high- and low-level clouds.

A study of MODIS CLWP uncertainties at high latitudes for mixed-phase clouds is presented by [78] with many instruments (i.e., AMSR-E, CloudSat, and CALIPSO). The results of multisensor CLWP retrievals show a CIWP-related CLWP bias, reaching almost 15% with CIWP of 150 g/m^2 and 40% or higher when CIWP is greater than 400 g/m^2 , in the case of mixed-phase clouds like liquid clouds. Furthermore, the unresolved angle-dependent bias of the solar zenith in MODIS CLWP, mainly caused by the variation in the cloud-top height due to three-dimensional radiative interactions with cloud-top inhomogeneity, is studied. It is possible to reduce the bias by 25 g/m^2 with a solar zenith angle of 80° and improve the agreement with AMSR-E CLWP trends by excluding only 0.5% of the data points that show significant errors.

It is possible to retrieve optical cloud properties and cloud height properties at the pixel level using the MODIS Level-2 cloud product (MOD06/MYD06 for Terra and Aqua MODIS, respectively); see [79]. Further information can be obtained with several product updates introduced in Collection 6. However, since the computations are considered to

yield baseline uncertainty due to sources of errors to the linear assumption inherent in the calculations, uncertainties on the order of 50% are expected to be of little value for science works. However, in single-layer cloud situations, ref. [80] find that the MODIS cloud algorithm produces cloud-top pressures within 50 hPa of lidar determinations.

In the case of optically thick clouds, ref. [81] demonstrated that ice cloud retrieval uncertainties in diurnal variation can be reduced by considering infrared measurements, temperature dependence, and ice particle habits.

The properties of ice-over-water were characterized by using the algorithm developed by [82]. The algorithm, which uses only the solar channels available on the MODIS and the Visible Infrared Imaging Radiometer Suite (VIIRS) sensors, is available for the case of an ice-over-water cloud with ice COT smaller than 7 and for an optically thicker liquid-water cloud (water COT > 5).

The methodologies for retrieving the effective diameter size and cloud optical thickness analyzed so far do not yield positive results for convective clouds with 3D morphology. Ref. [83] dedicate a study to this problem using MODIS, which includes channels in the shortwave IR with a single viewing angle, and the Multi-angle Imaging SpectroRadiometer (MISR), which provides multi-angle imagery in the visible and near-IR, MODIS. The combined use of both in the future should enable 3D retrievals of the effective size of cloud particles and extinction fields.

A similar study was conducted by [84], regarding the retrieval of cloud-top pressure and cloud-top height in the predominant multilayer regime of thin cirrus clouds above low clouds. They attempted to remedy the significant overestimation of the CTP and of cirrus emissivity via MODIS using the accuracy of low clouds' CTH retrieval through MISR. With this methodology, validated against Cloud-Aerosol Transport System (CATS) lidar observations, the average upper cloud CTP bias and emissivity are reduced by 90% and 75%, respectively, compared to standard MODIS products.

The MISR-MODIS synergy was also exploited by [85]. Using a full year of data (2013) and a variable ice particle roughness model, the authors investigated the retrieved ice cloud optical thickness, D_e , and CIWP over oceans under different conditions. In evaluating the annual cycles, this methodology provides a better understanding of the operational MODIS Collection 6 retrieved products.

Based on the Aqua MODIS and VIIRS SNPP products, the CLOUD PROPERTIES (CLD-PROP) product algorithms follow a "continuity of approach" paradigm for recording cloud properties. Given the strong scientific implications, ref. [79] illustrates details and impacts.

The problem with the lack of VIIRS IR absorption channels is discussed in the paper [86], in which a method to construct a water vapor and CO₂ IR channel for VIIRS with a spatial resolution of 750 m is suggested. Using the CALIPSO/CALIOP V4-20 cloud layer products and MODIS Collection 6.1 cloud-top products as a comparison, ref. [43] evaluates the cloud mask, cloud thermodynamic phase, and cloud-top height based on these constructed channels. The results indicate that each of the above cloud properties shows an improvement with the use of the constructed channel radiances. In particular, the value of the retrieved cloud-top height is comparable to the true cloud-top height measured using CALIPSO/CALIOP. Furthermore, it has been shown that the greatest improvement for the cloud mask occurs in the polar regions.

The potential for retrieving the cloud layer altitude, ice thickness, and frozen water path using the IASI and its successor IASI-NG is studied by [87]. For this purpose, cloud radiances were simulated with RTTOV and ECMWF profiles, and the amount and spectral distribution of ice cloud properties were determined using an analysis based on Shannon formalism. The results show a convergence rate of up to 95% for the requested products and expected errors that decrease with cloud opacity until signal saturation is reached.

The cloud retrieval algorithms analyzed so far generally provide reasonable estimates of cloud microphysical parameters under most conditions; however sun-glint areas remain a challenging problem. In the case where sunlight reflects off the water surface at the same angle as a satellite sensor views it, the sun glint can introduce a high degree of uncertainty in the retrieval of COT and CER [88]. Various approaches have been developed to model the sun glint radiance reflected by the sea surface, such as, for example, the Cox–Munk approach [89], which is based on statistical data [90]. The method described in [91] is also based on this approach, which yields good results in calculating the direct sun-glint radiance used in ocean color atmospheric correction. The problem of eliminating contamination from sun glint was also addressed by [92] through the development of an algorithm that uses the simultaneous determination of aerosols and wind speed.

A new frontier of innovation in the field of remote sensing has been provided by deep learning techniques, improvements in computational resources, and the growing quantity of satellite observations. Using convolutional neural networks, it is possible to consider statistical relationships between input variables and targets, capture spatial variations in input features, and reduce the computational load as well. Ref. [93] describes the retrieval of cloud-top height from MODIS with a neural network approach. The training database consists of cloud-top layer pressure data from the CALIOP dataset and brightness temperatures at 11 and 12 μm . The results show a mean absolute error (MAE) at least 32% (or 623 m) lower than the two operational cloud-top height reference algorithms (the MODIS Collection 6 Level 2 height product and the cloud-top temperature and height algorithm in the 2014 version of the NWC SAF—the EUMETSAT Satellite Application Facility on Support to Nowcasting and Very Short Range Forecasting—PPS (Polar Platform System)). The validation, carried out against both CALIOP and Cloud Profiling Radar (CPR, CloudSat), showed at least 32% (or 623 m) and 25% (or 430 m) MAE reductions, respectively.

SEVIRI measurements are the reference for the work on cirrus cloud detection and the retrieval of ice optical thickness, ice water path, and cloud-top height, developed by [94]. This paper describes the Cirrus Properties from SEVIRI (CiPS) NN algorithm, trained with SEVIRI infrared observations, CALIOP backscatter products, ECMWF surface temperatures, and other auxiliary data. A performance analysis of CiPS shows that the algorithm detects 71 and 95% of all cirrus clouds retrieved via CALIOP with an optical thickness of 0.1 and 1.0, respectively, and correctly classifies 96% of cirrus-free pixels. The cloud-top height retrieved via CiPS has a mean absolute percentage error of 10%, whereas, for the ice optical thickness, the mean absolute percentage error is 50%. Similar results are obtained for the ice water path.

An approach based on random forest (RF) machine learning techniques was tested by [95] for cloud mask and cloud thermodynamic-phase detection. For this purpose, two models were developed, using spectral observations from VIIRS on board the SNPP, and trained based on CALIOP data. The RF daytime model was evaluated over all surface types (TPR equal to 0.93 and higher, and FPR equal to 0.07 and lower), with the result that it performs the best among all models considered, including VIIRS CLDMSK and MODIS MYD35 products.

Machine learning-based techniques are applied to cloud CLWP retrieval in [96]. This topic is addressed based on SEVIRI data. The developed model was trained with CloudNet ground-based observation data and CLAAS-2 data as a high-quality reference. During the validation, this model achieved a higher correlation coefficient than physics-based retrieval in all situations.

Another aspect that can be addressed using machine learning algorithms is the estimation of CTH. This was done in the work of [97], where the combined use of active

and passive remote sensing measurements (CALIPSO cloud products and AHI radiance of Japanese GEO series) is proposed. Excellent results are obtained, with significant improvements in CTH for the mean absolute error (1.54–2.72 km).

Also in this area, ref. [98] propose an XGBoost machine learning (ML)-based model and describe a tool to retrieve cloud macrophysical parameters for Himawari-8 cloud detection, cloud-top height, and cloud-top temperature. This model, which can be used both day and night, provides more accurate results than the existing JAXA AHI cloud results; however, the retrieval accuracy still needs to be improved.

A deep learning approach that does not require auxiliary atmospheric parameters is developed by [99] to recover cloud properties, both day and night, from passive satellite observations. This method simultaneously recovers several cloud parameters (cloud optical thickness, cloud tops, cloud mask, the effective particle radius, and cloud height) involving convolutional neural network (TIR-CNN) thermal infrared radiances, viewing geometry and altitudes. The training database consists of MODIS products covering a full year, while the validation database is built with passive and active products observed in independent years. The cloud properties retrieved via TIR-CNN are found to be strongly consistent with all MODIS products.

Using the thermal infrared spectral channels of Himawari-8 and combining the machine learning technique with the radiative transfer model, ref. [100] obtained cloud detection and cloud microphysical properties with high spatio-temporal resolutions. The authors observed that, regarding cloud retrieval, this model performs better in sun-glint areas due to the overestimation of the official Himawari-8 products.

Creating coherent datasets on long-term cloud properties is the aim of ESA's (European Space Agency) Cloud Climate Change Initiative (Cloud_CCI) project based on AVHRR measurements. The study of [101] is the first to validate Cloud_CCI data products against ground instrument measurements from four high-latitude sites. The authors find that, although the Cloud_CCI CLWP retrievals are within ground-based instrument uncertainties, the Cloud_CCI Cloud Optical Depth (COD) turns out to be underestimated by about 3 optical depth (OD) units in the case of liquid-water clouds and by about 5 OD units if ice clouds are included. In the case of CTH, the observed overestimation becomes an underestimation of about 360–420 m for multilayer clouds.

A new version of the Pathfinder ATMOSpheres extended (PATMOS-x) multidecadal Cloud Properties Climate Data Record (CDR) is available from NOAA National Centers for Environmental Information (NCEI). Ref. [102] presents the new features introduced which concern the introduction of the HIRS 7.3- and 13.3- μm bands, the update of the previous values for the naive Bayesian detection scheme, and the improvement of cloud detection. The effects of these changes result in greater consistency in cloud-top height and phase distribution, as well as in polar cloud detection, when compared to MODIS EOS.

Table 2 summarizes the main information for each study reviewed in Section 2.2, the sensors and channels used, and the products investigated.

Table 2. Infrared observations-only recap table.

Authors	Year	Satellite		Main features	Uncertainty or Accuracy of the Method (When Declared/Applicable)
		Sensor	Channel Frequency [GHz]		
Fritz and Winston [34]	1962	-	-	Cloud properties	-
Smith and Platt [35]	1978	-	-	Cloud properties	-
Menzel et al. [36]	1983	-	-	Cloud properties	-
Eyre and Menzel [37]	1989	-	-	Cloud microphysics (i.e., particle size, COT)	-
Menzel et al. [38]	1990	-	-	Cloud microphysics (i.e., particle size, COT)	-
Minnis et al. [39]	1993	-	-	Cloud microphysics (i.e., particle size, COT)	$ACC_{OD,\%} \cong 25\%$
Nakajima and King [40]	1990	-	2.16, 3.7	COT, R_{eff}	-
Nakajima and Nakajima [42]	1995	AVHRR	3.75, 11	COT, R_{eff}	$RMSE_{COT,Reff,\%} < 25\%$
Han et al. [45]	1994	AVHRR	-	Cloud particle radii	-
Jolivet and Feijt [46]	2005	AVHRR	1.6	CLWP	$RMSE_{CLWP} = 28 \text{ g/m}^2$
Brenguier et al. [48]	2000	AVHRR	1.6	CLWP	-
Schüller et al. [49]	2003	AVHRR	1.6	Cloud properties	$RMSE_{CDNC} = 48.4 \text{ cm}^{-3}$
King et al. [50]	2004	AVHRR	1.62, 2.13	COT, R_{eff} , cloud phase	-
Kawamoto et al. [51]	2001	-	-	Cloud microphysics	-
Roebeling et al. [52]	2006	AVHRR, SEVIRI	1.6, 3.8	COT, CLWP, CPP	-
Pérez et al. [53]	2009	MODIS	-	R_{eff} , COT, CT	-
Iwabuchi et al. [54]	2016	MODIS	8.6, 10.4, 11.2, 12.4	CTH, COT, R_{eff} , CTP	$RMSE_{\%} < 30\%$
Iwabuchi et al. [55]	2018	AHI	-	CTH, COT, R_{eff} , CTP	-
Hanel et al. [56]	1972	IR sounder	-	Cloud microphysical properties	-
Smith et al. [57]	1993	IR sounder	-	Cloud radiative and microphysical properties	-
Kahn et al. [58]	2003	IR sounder	-	Cloud properties	-

Table 2. Cont.

Authors	Year	Satellite		Main features	Uncertainty or Accuracy of the Method (When Declared/Applicable)
		Sensor	Channel Frequency [GHz]		
Huang et al. [66]	2004	IR sounder	-	COT, effective particle size	$5\% < \text{RMSE}_{\text{COT},\%} < 20\%$
Wei et al. [60]	2004	AIRS	-	COT	-
Li et al. [67]	2005	AIRS, MODIS	-	Synergistic use of MODIS and AIRS cloud products	-
Zhou et al. [68]	2007	Ultra-spectral IR sounder	-	Cloud microphysical parameters	-
Liu et al. [69]	2009	IASI	-	Cloud properties	-
August et al. [70]	2012	IASI	-	Cloud detection, fractional coverage, height and phase	-
Martinet et al. [71]	2013	-	-	1D-Var assimilation system	-
Martinet et al. [73]	2014	IASI	-	1D-Var assimilation system	-
Wu et al. [76]	2017	IASI	-	Thin clouds	$\text{ACC}_{\text{CPH},\%} > 97\%$
Feofilov and Stubenrauch [77]	2017	AIRS	15	Cloud properties	-
Khanal and Wang [78]	2018	AMSR-E, CloudSat, CALIPSO, MODIS	-	Mixed-phase clouds	$\text{BIAS}_{\text{LWP,mixed clouds}} \cong 5.7 \text{ g/m}^2$
Platnick et al. [79]	2017	MODIS	-	Cloud-top and optical properties	-
Letu et al. [44]	2020	-	-	Cloud microphysical parameters	-
Menzel et al. [80]	2008	MODIS	-	Single-layer cloud-top pressure	-
Cox and Munk [89]	1954	-	-	Sunglint in cloud retrieval	-
King et al. [88]	1997	-	-	Sunglint in cloud retrieval	-
Nakajima and Tanaka [90]	1986	-	-	Sunglint in cloud retrieval	-
Wang and Bailey [91]	2001	-	-	Sunglint in cloud retrieval	-
Shi and Nakajima [92]	2018	-	-	Sunglint in cloud retrieval	-
Saito et al. [81]	2020	-	-	Optically thick clouds	-

Table 2. Cont.

Authors	Year	Satellite		Main features	Uncertainty or Accuracy of the Method (When Declared/Applicable)
		Sensor	Channel Frequency [GHz]		
Teng et al. [82]	2020	MODIS, VIIRS	0.4–0.7	Ice-over-water cloud properties	-
Forster et al. [83]	2021	MODIS, MISR	-	Convective clouds	-
Mitra et al. [84]	2023	MODIS, MISR	-	CTP, CTH in multilayer clouds	-
Wang et al. [85]	2019	MODIS, MISR	-	COT, R_{eff} , CTT, IWP	-
Weisz et al. [86]	2017	VIIRS, CrIS	-	-	-
Li et al. [43]	2022	VIIRS, CrIS	-	Cloud mask, cloud thermodynamic phase, CTH	-
Leonarsky et al. [87]	2021	IASI, IASI-NG	-	Cloud layer altitude, cloud thickness of ice	RMSE _{CBH} > 30%
Håkansson et al. [93]	2018	MODIS	-	CTH with neural network	-
Strandgren et al. [94]	2017	SEVIRI	-	Cirrus cloud properties (CTH, IOT, IWP)	-
Wang et al. [95]	2020	VIIRS	-	Cloud mask and thermodynamic-phase with random forest	-
Kim et al. [96]	2020	SEVIRI	-	CLWP with machine learning	BIAS _% = 9%
Min et al. [97]	2020	AHI, CALIPSO	-	CTH with machine learning	1.54 km < MAE _{CTH} < 2.72 km
Yang et al. [98]	2022	AHI	-	Cloud macrophysical parameters with XGBoost	RMSE _{CTH} = 18.67%
Wang et al. [99]	2022	MODIS	-	Cloud mask, COT, R_{eff} , CH, CTH with convolutional neural network	-
Tana et al. [100]	2023	AHI	-	Cloud microphysical properties combining RT model and machine learning	-
Vinjamuri et al. [101]	2023	AVHRR	-	Cloud products evaluation	-
Foster et al. [102]	2023	MODIS	-	PATMOS-x improved version	-

3. Combining Infrared and Microwave Observations

Exploiting the knowledge acquired so far, we can certainly state that IR and MW radiation are complementary. First, spaceborne radiometers detect IR radiation coming mainly from the top of the clouds, due to the strong absorption of IR wavelengths via cloud-forming hydrometeors, unlike MW radiation, which is only slightly affected as it passes through non-precipitating clouds. Furthermore, it is widely known that IR radiation is more responsive to small particles and rather low CIWP cirrus clouds. On the other hand, MW radiation is responsive to larger ice crystals and thicker cirrus cloud layers. These peculiarities of MW and IR radiation are schematically summarized in Figure 2, and they seem to suggest that a proper combination of MW and IR multispectral measurements could help determine the vertical structure and composition of clouds, especially in the case of multilayered clouds.

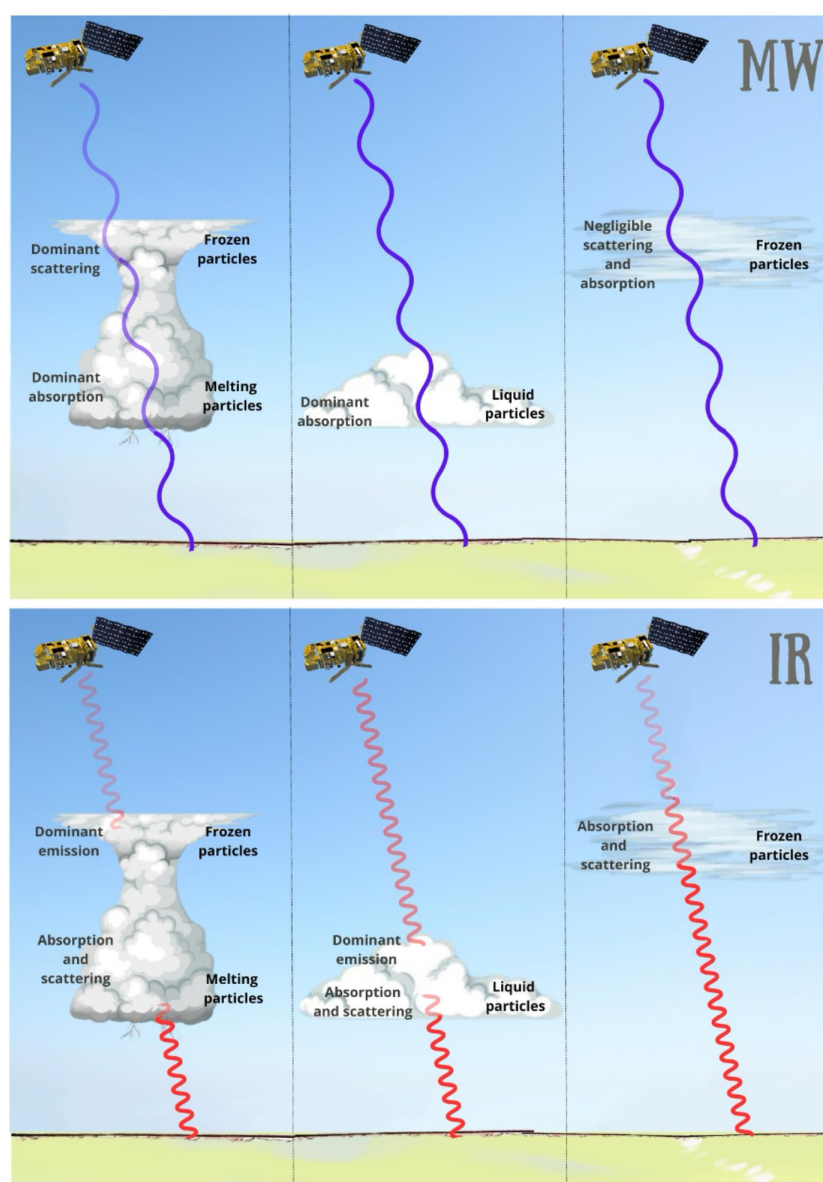


Figure 2. Sketches of the interaction between MW (**top**) and IR (**bottom**) radiation with thick convective cloud (**left**), low liquid cloud (**middle**), and cirrus cloud (**right**). Wave transparency indicates the radiation intensity after cloud interaction qualitatively. Also reported are the cloud phase and dominant cloud–radiation interaction (emission, absorption, and scattering).

In this context, ref. [103] proposed the new Microwave Visible and Infrared (MVI) technique. MVI allows the estimation of the frequency of multilayered clouds and the effective radius of droplets in water clouds, combining the possibility of deriving the CLWP and the water cloud temperature (T_w) from MW observations. This allows validation with radiosoundings and retrieval using a combined VIS and IR retrieval method. In [104], the authors reported the results of a series of tests on the MVI technique using Meteosat and SSM/I data collected in the framework of the Atlantic Stratocumulus Transition Experiment. The combination of satellite and ground-based radar data demonstrates the ability of the MVI technique to detect multilayered clouds, especially when low water clouds underlie higher ice clouds. The CLWP resulting from this method was evaluated against the corresponding product obtained from ground observation. The results show a correlation coefficient of 0.54 and a mean difference ground-based versus SSM/I CLWP estimation of 0.034 kg/m^2 or approximately 30% of the mean value with a maximum in the case of ground observations of locally high CLWP values ($>0.2 \text{ kg/m}^2$).

The benefits of the synergy between IR and MW are evident in the work of [105]. They address the cloud base height problem with a combination of MW observations from SSM/I and Special Sensor Microwave Water Vapor Sounder (SSM/T-2) on the Defense Meteorological Satellite Program (DMSP) satellite from a theoretical point of view. However, they find that only across the ocean is the signal strong. Retrieval over a significant range in CLWP improves significantly using the synergy of MW and IR data acquired from the same satellite (AMSU and AVHRR on NOAA-K). This is due to the ability to satisfy IR observations' cloud-top temperature constraint.

The potential for synergy between MW and IR is also clear in 1D-Var approaches, as in the paper of [106]. In this study, cloud-influenced observations are analyzed with a 1D-Var approach including both IR and MW sensors (HIRS/3 and AMSU-A aboard NOAA-15). A fast radiative transfer model, based on RTTOV 10.1 (see [72], Section 2.6.1), is presented, taking into account the specificities of both IR radiation (treating the cloud cover as a single semitransparent layer, defined by the cloud-top pressure and its effective amount) and MW (computing the cloud absorption from the profiles of cloud cover and liquid/ice water on any vertical pressure level). The developed scheme is tested with synthetic observations on individual profiles and in the real case of cloud retrieval from observations on 15 March 2001. In detail, the 1D-Var scheme is based on Advanced TOVS (ATOVS) observations. Consequently, IR radiances are always available when AMSU data are available; on the contrary, rain-affected MW data, if present, are removed consistently from the radiation model specifications, according to [107]. With respect to Clouds and the Earth's Radiant Energy System (CERES) Outgoing Longwave Radiation (OLR) observations, the 1D-Var retrieval scheme proves to be able to extract the liquid/ice water information contained in the radiances, showing clear improvements in the representation of the cloud ice model. On the other hand, MW information also has a positive impact on the knowledge of low clouds, while the representation of the vertical distribution of clouds needs to be improved due to the limits in the sensitivity of the passive IR and MW radiation. Unfortunately, as acknowledged by the authors themselves, the nonlinearity of cloud variation and the intrinsic on/off nature of cloud layers make the evaluation of the background-error covariance matrix rather problematic.

Combining near-IR, VIS, and MW observations from the Tropical Rainfall Measuring Mission (TRMM) satellite allowed [108] to develop a technique for drizzle detection in marine warm clouds. First, a near-IR/VIS algorithm is used to simultaneously identify COT and the effective radius; then, CLWP is retrieved via a new algorithm developed in MW. Simulations from radiative transfer models supported by the analysis of satellite observations allowed the study of the relationship between OD, the effective radius, and

CLWP, whereas radar observations of clouds in coincident areas constituted the validation dataset of the described method.

Observations in the MODIS bands, combined with the AMSR-E frequencies, allow for the estimation of CLWP and CIWP for double-layer clouds. This topic was addressed by [109]. They developed a method to evaluate the CLWP of lower-layer water clouds from AMSR-E observations and, subsequently, the properties of upper-level ice clouds from MODIS by matching the radiances simulated by an RTM with a two-cloud layer. This approach can achieve COT and CIWP retrievals with significantly improved accuracy and reduced overestimation for ice-over-water cloud systems, as indicated by comparisons with single-layer cirrus systems and surface-based radar retrievals.

The development of new techniques to improve the retrieval of cloud parameters, especially in the presence of multilayered clouds, is also required, given the evidence that methods that usually provide accurate results in the case of a single cloud layer (such as, for example, the CO₂ slicing technique for cloud-top retrieval or IR-only observations for cloud properties retrieval) are not reliable in the case of thick clouds with multiple layers. In these cases, the approach developed by [110], which uses multispectral satellite data (AIRS and AMSU) to penetrate the cloud-top, can be useful to obtain reliable data and a better agreement with ground-based observations. The validation work considered 40 ground observations collected at the Chilbolton Observatory Facilities (UK) during spacecraft flybys and found an RMS agreement within 295, 905, 1094, and 1862 m for CTH and CBH, and 0.62, 0.08, and 0.02 kg/m² for TPW, CLWP, and CIWP, respectively. These results lead to the conclusion of a better ability for HIRS to discriminate between ice/no-ice clouds than AMSU-A or MHS.

The synergistic use of observed data from different sensors requires careful collocation work. The development of a simpler collocation methodology between the MHS on board NOAA-18 and the CPR on board CloudSat is the subject of the paper by [111]. In addition to the description of this new collocation-finding method, the paper presents the results and statistical analyses performed and a section dedicated to the practical implications. The validation of the operational CIWP product from MHS measurements, the NOAA MSPPS, against CloudSat CIWP highlights a low sensitivity found in many null values for the MSPPS CIWP, probably due to thin clouds' being rather transparent at MHS frequencies. To overcome this, the authors also evaluate the addition of two HIRS channels (8 and 11) to the CIWP retrieval from MHS. This, however, leads to only a small detectable improvement for small values of CIWP due to modest improvements in the HIRS-MHS footprint difference and beam-filling issues.

An interesting result regarding the synergy between IR and MW is obtained by [112], which, for the case examined, does not agree with the most widespread conclusions on this topic. In fact, by applying an approach based on the Support Vector Machine (AID-SVM) methodology and on information ice/no-ice clouds acquired via the CloudSat CPR, the paper highlights that this methodology offers very promising potential to obtain information on ice clouds/no ice using passive satellite sensors, over both the ocean and the land surface. However, in the cases studied, it appears that IR satellite sensors, such as HIRS, are more efficient at detecting ice clouds than MW satellite sensors and that combined measurements using MW/IR synergy do not perform better than IR measurements alone. The method was applied and tested on data from various sensors (AMSU-A, MHS, and HIRS instruments aboard NOAA-19 satellite) providing an ice cloud detection probability of 0.37 for AMSU/A, 0.51 for MHS, 0.83 for HIRS, and 0.83 for the AMSU/A, MHS, and HIRS combination over the ocean. Similarly, over land, the authors obtain 0.42 for AMSU/A, 0.50 for MHS, 0.76 for HIRS, and 0.80 for AMSU/A + MHS + HIRS.

Ref. [113] addresses the problem of atmospheric ice detection and the CIWP retrieval completely based on passive operational sensors Synergistic Passive Atmospheric Retrieval Experiment-ICE (SPARE-ICE). They develop a set of NN trained on an observation-based dataset of AVHRR and MHS measurements on the one hand and joint radar–lidar CIWP on the other hand, obtained by collocating NOAA-18 with the Cloudsat and CALIPSO Ice Cloud Property Product (2C-ICE) CIWP product. The algorithm, which exploits three AVHRR channels, three MHS channels, and auxiliary information such as satellite angles, surface temperature, and surface elevation, reveals a very good correlation for $CIWP > 10 \text{ g/m}^2$ between the reference dataset 2C-ICE and SPARE-ICE. For smaller values of CIWP, SPARE-ICE shows the tendency to be larger than 2C-ICE, becoming stable at a median of about $1\text{--}2 \text{ g/m}^2$ for 2C-ICE $CIWP < 1 \text{ g/m}^2$. Furthermore, the paper indicates that SPARE-ICE is not sensitive to small values of CIWP. Unfortunately, it was not possible to provide a direct estimate of uncertainty for a single retrieval using NN. However, an error estimate as a function of CIWP was provided based on the validation dataset, i.e., data not used in the training phase. Based on the fractional error definition, the authors found a value of about 2 between SPARE-ICE and CloudSat 2C-ICE for the median fractional error, comparable to the random error between 2C-ICE and in situ CIWP measurements.

The advantages of combined retrieval are also addressed in the work of [114]. In this study, the improvements to the AIRS/AMSU version 6 retrieval algorithm are explored. Flying on the same satellite platform (Aqua), the AIRS and AMSU instruments lend themselves very well to evaluating the trend of combined retrievals. This algorithm is now operational at the NASA Goddard Data and Information Services Center (DISC). Since September 2002, Level 2 and Level 3 products have been available, and, in particular, AIRS Science Team version-6, level-2 products can be accessed in near real time on the Goddard DISC. The initial state underlying the operation of the algorithm is generated from the AMSU and AIRS observations, also providing the set of values of the variables that characterize the clouds (radiatively effective cloud fraction and cloud-top pressure), as well as supporting the actual physical retrieval procedure. In detail, compared to the previous operational version, the improvements contained in the AIRS Science Team version-6 retrieval algorithm are many and significant, and they also include the methodology for determining the cloud parameters, which are retrieved from up to two layers of gray clouds in a given scene. Furthermore, in version 6, there is the possibility that the algorithm can also work in AIRS-only (AO) mode. This processing mode uses exclusively AIRS observations without benefiting from the contribution of AMSU observations in any phase, including the generation of the version-6 AO initial state. The ability to operate in AO mode is extremely important, as it provides a backup if AMSU information deteriorates significantly. From a quality perspective, version-6 AO retrievals are generally only slightly less accurate than those of the full version 6. The main differences between the results of the two modes are mostly found over the ocean, as AO mode cannot benefit from observations in the 22 and 31 GHz channels of AMSU-A.

Another algorithm based on AIRS-like sounding systems is the NOAA Unique Combined Atmospheric Processing System (NUCAPS), which has its origin in the AIRS Science Team approach [114]. This algorithm, designed at the NOAA National Environmental Satellite, Data, and Information Service (centre) for Satellite Applications and Research (NOAA/NESDIS/STAR), and the underlying spectroscopy are currently used to process data from combined MW and IR channels of the AIRS/AMSU suite, the IASI/AMSU/MHS suite (operational since 2008) and, more recently, the Cross-track Infrared Sounder (CrIS)/ATMS suite, operational since 8 April 2014. It was designed with a modular architecture, and the objective of some of the six modules (modules 2, 3, 5, and 6) of which it is composed is precisely the retrieval of cloud properties, based on the synergy of

data from MW and IR. In more detail, based on MW-only observations, cloud liquid-water flags and surface emissivity uncertainty (module 2), as well as temperature and moisture variables, are recovered via an all-sky eigenvector regression approach (module 3), a second fast eigenvector regression retrieval for temperature and moisture for cloud cleared radiances (module 5), and a final IR physical retrieval, with the previous regression retrieval as the first guess (module 6). The remaining modules are dedicated to quality control for the input, search tables, and acquisition of accessory products (module 1) and to obtaining a cloud clearing module that combines a set of MW and IR channels (module 4). NUCAPS, which came into operation in April 2018, has been the subject of numerous studies that have validated its performance (i.e., [115]).

The synergy of ground-based, high-resolution IR and MW observations was studied by [116] in the case of thin clouds of single-layer liquid water ($CLWP < 0.1 \text{ kg/m}^2$). In these situations, MW observations have generally lower sensitivity than in other cases, unlike IR observations, which show higher sensitivity. The developed methodology relies on an NN scheme to estimate both CLWP and cloud-effective radius, based on a synthetic dataset of MW observations and additional broadband and highly spectrally resolved IR observations. The results show that the NNs can retrieve CLWP and D_e with a mean relative error of 9% (for CLWP) and 17% (for D_e). Consistently with the sensitivity of MW observations in the case of thin clouds, the retrieval is affected by a high relative error, using only MW data, contrary to what is observed for IR retrievals ($CLWP 40\text{--}60 \text{ g/m}^2$). As a result, combined (MW with broadband IR observations) retrievals are affected by less error than MW alone. Furthermore, the addition of the high-resolution IR spectrometer further decreases the relative error by 5% (CLWP) and 7% (D_e), compared to the results with the broadband IR radiometer.

A methodology addressing the correction of cloud liquid water path (CLWP) measurements provided via Geostationary Operational Environmental Satellites-R (Series) (GOES-R) Advanced Baseline Imager (ABI) observations using microwave CLWP was developed by [117]. The CLWP ABI duly corrected for errors due to the scattering geometry and low cloud fraction showed significantly better reliability, especially at dawn and dusk and in non-rainy conditions.

The problem of the combined use of Microwave Sounder (MWS) observations and future infrared (IASI-NG) observations for cloud liquid and ice water path retrieval has been addressed by [118]. The authors propose an NN approach that, while also considering the impact of next-generation sensors, can lead to notable improvements (up to 20%).

Pairs of infrared and microwave instruments on Aqua, Suomi-NPP, and NOAA-20 provide observations for the Community Long-term Infrared Microwave Combined Atmospheric Product System (CLIMCAPS) products. Ref. [119] describes three-decade research conducted by the NASA AIRS Science Team (NASA AST) to retrieve profiles of atmospheric temperature, water vapor, ozone, and many other trace gases, as well as cloud (cloud liquid water, cloud-top pressure, and cloud fraction) and surface properties.

A new application can be found in [120]. In this recent study, the authors developed a highly performing retrieval technique for ice hydrometeors. This methodology, which is based on neural network applications, exploits the sensitivity of submillimeter waves (in synergy with IR spectra) to the scattering effects of ice crystals. The retrieval of CIWP and D_e was evaluated through a sensitivity analysis using a simulated synthetic dataset. The obtained results are very encouraging, and they demonstrate that a synergistic strategy can improve the retrieval accuracy with mean square error values that are 68% (95%) and 10% (24%) lower for CIWP and D_e , respectively, compared to the corresponding retrievals using sub-mm only (IR-only).

Table 3 summarizes the main information for each study reviewed in Section 3, the sensors and channels used, and the products investigated.

Table 3. IR–MW-combined observations recap table.

Authors	Year	Satellite		Main Features	Uncertainty or Accuracy of the Method (When Declared/Applicable)
		Sensor	Channel Frequency [GHz]		
Lin et al. [103]	1998	SSM/I, SEVIRI	-	Multilayered CF and R_{eff} with MVI technique	-
Albrecht et al. [104]	1995	SSM/I, SEVIRI	-	Atlantic Stratocumulus Transition Experiment	-
Wilheit and Hutchison [105]	2000	AMSU, AVHRR	-	CLWP	-
Chevallier et al. [106]	2002	AMSU-A, HIRS/3	-	1D-Var approach for cloud-affected BT	-
Saunders et al. [72]	2012	-	-	RTTOV	-
Zhao et al. [107]	2000	-	-	1D-Var scheme with rain-affected MW BT detection	-
Shao and Liu [108]	2004	TRMM	IR, VIS, MW	Drizzle in marine warm clouds, COT, R_{eff} , CLWP	-
Huang et al. [109]	2006	MODIS, AMSR-E	-	upper-level ice cloud properties	$\text{RMSD}_{\text{IWV},\%} = 9\%$
Romano et al. [110]	2007	AIRS, AMSU	-	Retrieval of multi-layer cloud parameters	-
Holl et al. [111]	2010	MHS, CPR, HIRS	-	CIWP	-
Islam et al. [112]	2014	AMSU-A, MHS, HIRS	-	Ice cloud detection	$0.88 < \text{ACC} < 0.93$
Holl et al. [113]	2014	AVHRR, MHS	-	CIWP	$\text{MFE}_{\text{SPARE-ICE}} = 100\%$
Susskind et al. [114]	2014	AIRS, AMSU	-	Cloud properties	-
Marke et al. [116]	2016	-	-	Liquid-water cloud microphysical properties	$2.4 \text{ g/m}^2 < \text{RMSE}_{\text{LWP}} < 9.1 \text{ g/m}^2$
Nalli et al. [115]	2013	AIRS, AMSU, IASI, MHS, CrIS, ATMS	-	NUCAPS algorithm validation	-
Smalley and Lebsack [117]	2023	ABI	-	LWP	$20 \text{ g/m}^2 < \text{RMSE}_{\text{LWP}} < 40 \text{ g/m}^2$
Cimini et al. [118]	2023	IASI-NG, MWS	-	CLWP and CIWP with neural network	-
Smith and Barnett [119]	2023	IR and MW instruments pairs	-	CLIMCAPS products	-

4. Cloud Parameter Databases and Retrieval Methods

The retrieval of cloud parameters is a topic that has always interested the scientific community working in the field of Earth science, and numerous projects have been dedicated to it since the 1980s. Among the first in chronological order, there is certainly the International Satellite Cloud Climatology Project (ISCCP) described by [121]. This project aimed to provide some data of interest for cloud (optical thickness and top pressure) from 1983 to 2009. PATMOS-x also deals with operational processed cloud retrieval by providing a complete suite of atmospheric and cloud products based on observations from the AVHRR sensor flying on polar-orbiting weather satellites since the late 1970s. PATMOS-x was developed at NOAA/NESDIS/STAR in collaboration with the University of Wisconsin and Madison Cooperative Institute for Meteorological Satellite Studies (CIMSS) and is described by [122].

AVHRR data recorded on board the PM satellites of the NOAA Polar Operational Environmental Satellite (POES) missions are collected in the 35-year (1982–2016) climatological Cloud_CCI Advanced Very High Resolution Radiometer post meridiem (AVHRR-PM) dataset (version 3), containing global cloud and radiation properties on a grid with a latitude–longitude resolution of 0.05° (details in [123]). The CM SAF cCloud, Albedo and surface RAdiation dataset from AVHRR data (CLARA) dataset is a global dataset containing surface radiation products and data on surface albedo, as well as cloud properties, generated via the EUMETSAT CM SAF. Its first version (CLARA-A1) is based on AVHRR measurements recorded in polar orbit onboard the NOAA and MetOp satellites. The data cover a 28-year period (1982–2009) and are arranged on a regular global grid with a resolution of 0.25 degrees (latitude–longitude). More details can be found in [124].

The CLARA-A1 dataset has been updated to CLARA-A2, the second edition, described in [125]. The reference time is extended to 34 years, reaching up to 2015.

As regards clouds, the averaged products are available with two temporal samples (daily and monthly), while, as global products, a daily resampling is available for individual satellites. The dataset contains the cloud mask, cloud-top temperature/pressure/height, cloud thermodynamic phase, and cloud optical thickness, particle effective radius, and cloud water path. Spatially, the monthly and daily averages are available on a global $0.25^\circ \times 0.25^\circ$ grid. Furthermore, for the polar regions, cloud products are also provided in two equal $25 \text{ km} \times 25 \text{ km}$ grids.

The v.4 retrieval algorithms for CERES–MODIS products were implemented from 2012 until MODIS data were available at a resolution of $1^\circ \times 1^\circ$ (latitude by longitude). CERES aims to study Earth's climate system to analyze the role of cloud and radiation feedback [126]. During this study, the following cloud product retrievals were obtained: ice water path, liquid-water path, cloud particle phase, cloud base pressure, cloud-top pressure, ice particle effective diameter, water particle radius, and cloud visible optical depth [127].

As mentioned above, the MOD06 and MYD06 databases for Terra and Aqua, based on level 2 (L2) MODIS products, provide pixel-level retrievals of optical properties of clouds (optical thickness, effective particle radius, CLWP, CIWP, and thermodynamic phases—daytime only) and cloud-top properties (temperature, pressure, and height—both day and night). An overview of the major updates contained in the latest reprocessing (MOD06 C6 of 2000 and MYD06 of 2002, respectively) is outlined in [79].

Although the methodologies underlying the cloud product dataset and ancillary data may vary from case to case, clear sky reference data and cloud radiance simulations are typically produced using radiative transfer models. The solution of the inverse problem is another important aspect in these techniques that, in most of them, is addressed by searching in a large look-up table (LUT) for the value/parameter that best fits the radiances

observed in the different spectral bands. The most widespread approach in the inversion procedure is based on the optimal estimation method (OEM) described by [74], in which attempts are made to maximize the probability of the retrieved state, conditional on the value of the measurements and any a priori knowledge. This is an iterative procedure in which convergence is sought by varying the first guess at each interaction [128].

Statistical techniques such as NN, deep learning (DL), and CNN have been widely applied to retrieve cloud parameters from satellite measurements [99,118,129,130], proving, in some cases, to be an excellent alternative to variational retrieval, which is generally more expensive from a computational point of view. While neural networks are well suited to investigating the full nonlinearity of measurements, it is worth remembering that the NN itself is a statistical model. This makes it susceptible to similar problems associated with retrievals based on linear statistics. Estimating the error associated with network output is a rather complicated task, which is why physical retrieval is typically preferred, since it allows one to easily estimate the error by means of the covariance associated with the output [74]. Regarding the assessment of errors associated with the output of an NN, these are typically estimated on the basis of the total root mean square error (RMSE) evaluated on the training dataset. However, although reasonable in a linear case, this approach is not entirely satisfactory, as it does not allow for evaluating the error bars for the single output. As a result, the performance of the algorithm is not represented correctly if the performance is expected to degrade over a given range of input variables.

Potential synergies between two or more datasets from independent observations of the same target offer important implications in the field of remote atmospheric sounding. For this reason, more and more attention is being paid to the study of optimized or innovative methods to combine two or more measured datasets. For example, a synergistic approach can be developed by applying an appropriate retrieval scheme that involves feeding multi-wavelength observations into a single input and then performing a simultaneous inversion of all observations, or via an a posteriori combination of stand-alone retrieval products from individual measurements. Ref. [131] compared these two strategies for data fusion in the case of multi-wavelength remote sensing observations and demonstrated the better performance of the synergistic inversion scheme. Applications for retrieving atmospheric profiles from IASI, MHS on MetOp-A, and AMSU-A are shown.

The cloud masking problem has been addressed with several approaches, such as naive Bayes in PATMOS-x, threshold test sequences in MODIS C6 or some dynamic thresholding in CLARA. Cloud phase retrieval has also been addressed in the literature with several techniques. For example, it is determined as a function of a combined test between different channels and the cloud-top temperature in CLARA, whereas [132] describe a threshold algorithm in PATMOS-x. Refs. [133,134] use a combination of four CTT-based tests, three infrared channels, 1.38 μm , and cloud-effective data in MODIS C6. The cloud-effective data considered in [133,134] include the cloud-effective radius, the effective temperature and the effective cloud amount defined as cloud fraction multiplied by cloud emissivity. The method developed by [40], however, is usually used to calculate the cloud-effective radius and cloud optical thickness.

Furthermore, many retrieval algorithms have been evaluated/validated in several studies. Ref. [135] estimated the deviation between the collocated MYD06 product and the MODIS-based PATMOS-x microphysical retrievals. In this case, good results were obtained, with output within the retrieval uncertainty. Instead, for CLARA-A2, the global CTH is underestimated by 840 m compared to the measurement of the active sensor Cloud-Aerosol Lidar with Orthogonal Polarization (CALIOP). Ref. [125] compared CLARA-A2 with PATMOS-x and MODIS C6 products and found that the cloud-top pressure of CLARA-A2 is 4–90 hPa lower and quantified the absolute cloud phase bias as lower than 9%. Finally,

the bias of MODIS C6 CTH compared to CALIOP for low-level boundary layer water clouds is +197 m.

5. Summary and Conclusions

Currently, most attempts to derive cloud microphysical properties from satellite observations involve the disjointed use of MW and IR measurements, which are only subsequently integrated. In this review, we have addressed the problem of developing algorithms that simultaneously/hierarchically combine all the complementary information obtained from different spectral ranges. As described, the importance of strategies for integrating data acquired at MW, IR and VIS wavelengths has emerged as a powerful resource for improving microphysical cloud-parameter retrieval products. The development of methodologies and algorithms to fully exploit the synergistic content of the information carried via the different bands creates exciting opportunities to improve our understanding of cloud-scale microphysical variables, the hydrogeological cycle, and moisture redistribution. This review paper has covered the fundamental aspects of cloud interaction with MW and IR radiation and provided a comprehensive overview of the current state of retrieval algorithms, considering methodologies that derive cloud properties from IR and MW satellite observations separately and in synergy. The review raised the following considerations.

5.1. Importance of Understanding Cloud Microphysical Properties at Different Spatial/Temporal/Scales

Clouds constitute the largest uncertainty in current general circulation models. There are reliable observation methods that accurately measure their main parameters at the microphysical scale. However, the representation of clouds can be further improved by better understanding the microphysical processes. In this perspective, a largely unexploited potential for the retrieval of cloud properties, such as the cloud drop effective radius, the cloud liquid, and ice water contents and their column-integrated values, is represented by the synergy of infrared and microwave observations. The results reviewed in this paper show that this synergy reduces the error in cloud microphysical parameters retrieved from satellite measurements.

5.2. IR and MW Peculiarities

Infrared and microwave observations exhibit numerous differences in spectroscopic properties, propagation through clouds, and surface emission characteristics, providing highly complementary information to each other. In general, from the perspective of measuring the microphysical cloud properties, the algorithms based on MW observations exploit frequencies at 23.8, 31.4, 90, and 183 GHz to obtain information on atmospheric water vapor and liquid water contained in a cloud, while the 88–90 and 150–205 GHz channels are mainly used in approaches to study ice clouds and precipitation. On the other hand, passive infrared observations show sensitivity to liquid and ice particles closer to the top of the clouds within the observed volume. The strategies in the case of infrared channels are mainly based on radiance measurements, which also allow the retrieval of the cloud optical thickness and effective cloud particle diameter. The results reviewed in this paper quantifiably show that, although microwaves are less sensitive to clouds than infrared, higher sensitivity to cloud microphysical properties is achievable using higher frequencies.

5.3. Evolution of Observing Technology and Data Analysis Techniques

The increase in spatial/spectral/temporal resolution of sensors planned for the coming years promises significant improvements in the performance of retrieval algorithms. However, apart from sensor technology, other aspects are becoming increasingly important for cloud observations. This is the case for the evolution of time series analysis techniques

and approaches based on new methodologies, such as artificial intelligence and machine learning, that can now count on consolidated multi-year datasets and increasingly high-performance computing power. In compiling this review, we found an increasing number of approaches based on these new methodologies. The reviewed results indicate significant improvement in accuracy, paving the road for more accurate cloud microphysics products and new knowledge in the future.

To further highlight the benefits of synergistic over IR/MW-only approaches, we have summarized the results from the ComboCloud project (funded by EUMETSAT), which aimed to retrieve essential cloud parameters by exploiting the combination of innovative features offered via upcoming satellite sensors, along with the synergy between IR and MW measurements. The improvements that can be expected concern both CLWP and CIWP and are about 2–14% and 4–8%, respectively, for correlation. Similarly, a gain of a factor of 1.4–2.4 and 1.7–2.1, respectively, is certified in the case of RMSE.

Author Contributions: Conceptualization, M.V. and F.R.; supervision, M.V., S.T.N., F.R., and D.C.; visualization, S.T.N.; writing—original draft preparation, M.V., D.C., and F.R.; writing—review and editing, M.V., F.R., D.C., S.T.N., F.D.P., D.G., S.L., M.P.D.N., and D.M. All authors have read and agreed to the published version of the manuscript.

Funding: Part of this research was funded by EUMETSAT through the ComboCloud project (www.eumetsat.int/combocloud,EUM/CO/19/4600002352/THH). The authors also acknowledge the support of the Italian Ministry of University and Research and Next Generation EU through the study/project SnowMed (PRIN 2022 Prot. 2022Z2KTJ4).

Data Availability Statement: No new data were created or analyzed in this study. Data sharing is not applicable to this article.

Conflicts of Interest: The authors declare no conflicts of interest. The funders played no role in the design of the study, in the collection, analyses, or interpretation of data, in the writing of the manuscript, or in the decision to publish the results.

Abbreviations

Abbreviation	Meaning
2C-ICE	Cloudsat and CALIPSO Ice Cloud Property Product
AATSR	Advanced Along-Track Scanning Radiometer
ABI	Advanced Baseline Imager
AHI	Advanced Himawari Imager
AIRS	AtmoSphericAtmospheric InfraRed Sounder
AMSRE	Advanced Microwave Scanning Radiometer for EOS
AMSU	Advanced Microwave Sounding Unit
AO	AIRS-Only
ARM	(US Department of Energy) Atmospheric Radiation Measurement (user facility)
ARTS	Atmospheric Radiative Transfer Simulator
ATMS	Advanced Technology Microwave Sounder
ATOVS	Advanced TOVS
AVHRR	Advanced Very High Resolution Radiometer
AVHRR-PM	AVHRR-Post Meridiem
BT	Brightness Temperature
BTD	Brightness Temperature Differences
CALIOP	Cloud-Aerosol Lidar with Orthogonal Polarization

CALIPSO	Cloud-Aerosol Lidar and Infrared Pathfinder Satellite Observation
CATS	Cloud-Aerosol Transport System
CBH	Cloud Base Height
CDR	Climate Data Record
CERES	Clouds and the Earth's Radiant Energy System
CIMSS	Cooperative Institute for Meteorological Satellite Studies
CiPS	Cirrus Properties from SEVIRI
CIRS-LMD	Clouds from InfraRed Sounders, developed at LMD
CIWC	Cloud Ice Water Content
CIWP	Cloud Ice Water Path
CLAAS-2	CM SAF Cloud Property Dataset using SEVIRI-Edition 2
CLDMSK	CLouD MaSK
CLDPROP	CLouD PROPERTIES
CLIMCAPS	Community Long-term Infrared Microwave Combined Atmospheric Product System
CLIWA-NET	Cloud LIquid WATER NETwork (project)
Cloud_CCI	Cloud Climate Change Initiative
CLWC	Cloud Liquid Water Content
CLWP	Cloud Liquid Water Path
CM SAF	Satellite Application Facility on Climate Monitoring
CNRS	Centre National de la Recherche Scientifique
COD	Cloud Optical Depth
COT	Cloud Optical Thickness
CPP	Cloud Physical Properties
CPR	Cloud Profiling Radar
CrIS	Cross-track Infrared Sounder
CSU	Colorado State University
CTH	Cloud-Top Height
CTP	Cloud-Top Pressure
CTT	Cloud-Top Temperature
DARDAR	raDAR/liDAR
D_e	(cloud) Drop effective diameter
DISC	Data and Information Services Center
DL	Deep Learning
DMSP	Defense Meteorological Satellite Program
ECMWF	European Centre for Medium-Range Weather Forecasts
EOF	Empirical Orthogonal Function
EOS	Earth Observing System
ESA	European Space Agency
EUMETSAT	EUropean organisation for the exploitation of METeorological SATellites
FOV	Field Of View
FPR	False Positive Rate
FY-3	FengYun-3
GDAS	Global Data Assimilation System
GEO	GEOstationary (orbit satellite)
GFS	Global Forecasting System
GOES-R	Geostationary Operational Environmental Satellites-R (Series)
HIRS/3	High-resolution Infra Red Sounder/3
HIS	Hyperspectral Imaging Sensor
HSB	Humidity Sounder for Brazil

IASI	Infrared Atmospheric Sounding Interferometer
IASI-NG	IASI-Next Generation
ICAS	Integrated Cloud Analysis System
ICON-NWP	ICOsahedral Nonhydrostatic NWP
IPCC AR6	Intergovernmental Panel on Climate Change—Sixth Assessment Report
IR	InfraRed
ISCCP	International Satellite Cloud Climatology Project
IWV	Integrated Water Vapour
JAIVEx	Joint Airborne IASI Validation EXperiment
JAXA	Japan Aerospace Exploration Agency
LMD	Laboratoire de Meteorologie Dynamique (CNRS, Paris)
LUT	Look Up Table
MAE	Mean Absolute Error
MAS	MODIS Airbone Simulator
MHS	Microwave Humidity Sounder
MIRS	Microwave Integrated Retrieval System
MISR	Multi-angle Imaging SpectroRadiometer
ML	Machine Learning
MLP	MultiLayer Perceptron
MMW	MilliMeter-Wave scanning radiometers
MODIS	MODerate resolution Imaging Spectroradiometer
MR	Minimum Residual
MSG	Meteosat Second Generation
MSPPS	Microwave Surface and Precipitation Products System
MVI	Microwave Visible and Infrared
MW	MicroWave
MWI	MicroWave Imager
NASA	National Aeronautics and Space Administration
NASA AST	NASA AIRS Science Team
NASA GPROF	NASA Goddard Profiling Algorithm
NCEI	National Centers for Environmental Information
NN	Neural Network
NOAA	National Oceanic and Atmospheric Administration
NOAA/NESDIS/STAR	NOAA National Environmental Satellite, Data, and Information Service (centre) for SaTellite Applications and Research
NUCAPS	NOAA Unique Combined Atmospheric Processing System
NWC SAF	Satellite Application Facility on support to NoWCasting and Very Short Range Forecasting
NWP	Numerical Weather Prediction
OD	Optical Depth
OEM	Optimal Estimation Method
OLR	Outgoing Longwave Radiation
OSSE	Observing-System Simulation Experiments
PATMOS-x	Pathfinder ATMOSpheres extended
PCRTM	Principal Component-based Radiative Transfer Model
POES	Polar Operational Environmental Satellite
PPS	Polar Platform System
R	Correlation coefficient
RF	Random Forest
RMS	Root Mean Square
RMSD	Root Mean Square Differences
RMSE	Root Mean Square Error
RTTOV	Radiative Transfer for TOVS

RTTOVCLD	RTTOV ClouD (interface)
SEVIRI	Spinning Enhanced Visible and InfraRed Imager
SNPP	Suomi National Polar-orbiting Partnership
SPARE-ICE	Synergistic Passive Atmospheric Retrieval Experiment-ICE
SSM/I	Special Sensor Microwave/Imager
SSMIS	Special Sensor Microwave Imager/Sounder
SVM	Support Vector Machine
TEMPEST-D	Temporal Experiment for Storms and Tropical Systems Technology-Demonstration
TIR	Thermal InfraRed
TIR-CNN	Convolutional Neural Network Thermal Infra
TIROS	Television InfraRed Observation Satellite
TMI	Tropical Rainfall Measurement Mission Microwave Imager
TOVS	TIROS Operational Vertical Sounder
TPR	True Positive Rate
TPW	Total Precipitable Water
TRMM	Tropical Rainfall Measuring Mission
TROPICS	Time-Resolved Observations of Precipitation structure and storm Intensity with a Constellation of Smallsats
T_w	Temperature of cloud water
VIIRS	Visible Infrared Imaging Radiometer Suite
VIS	Visible
σ	Uncertainty

References

1. IPCC: *Climate Change 2022—Impacts, Adaptation and Vulnerability: Working Group II Contribution to the Sixth Assessment Report of the Intergovernmental Panel on Climate Change*, 1st ed.; Cambridge University Press: Cambridge, UK, 2023. [CrossRef]
2. Ricciardelli, E.; Cimini, D.; Di Paola, F.; Romano, F.; Viggiano, M. A statistical approach for rain intensity differentiation using Meteosat Second Generation—Spinning Enhanced Visible and InfraRed Imager observations. *Hydrol. Earth Syst. Sci.* **2014**, *18*, 2559–2576. [CrossRef]
3. Di Paola, F.; Casella, D.; Dietrich, S.; Mugnai, A.; Ricciardelli, E.; Romano, F.; Sanò, P. Combined MW-IR Precipitation Evolving Technique (PET) of convective rain fields. *Nat. Hazards Earth Syst. Sci.* **2012**, *12*, 3557–3570. [CrossRef]
4. Romano, F.; Cimini, D.; Di Paola, F.; Gallucci, D.; Larosa, S.; Nilo, S.T.; Ricciardelli, E.; Iisager, B.D.; Hutchison, K. The Evolution of Meteorological Satellite Cloud-Detection Methodologies for Atmospheric Parameter Retrievals. *Remote Sens.* **2024**, *16*, 2578. [CrossRef]
5. NASA, Global Precipitation Measurement: IMERG: Integrated Multi-satellitE Retrievals for GPM. Available online: <https://gpm.nasa.gov/data/imerg> (accessed on 18 January 2025).
6. Heinemann, T.; Kernyi, J. *The EUMETSAT Multisensor Precipitation Estimate (MPE): Concept and Validation*; EUMETSAT: Darmstadt, Germany, 2004; p. 8. Available online: https://www-cdn.eumetsat.int/files/2020-05/mpe_conceptvalidation_uc2003.pdf (accessed on 18 January 2025).
7. Eyre, J.R.; English, S.J.; Forsythe, M. Assimilation of satellite data in numerical weather prediction. Part I: The early years. *Q. J. R. Meteorol. Soc.* **2019**, *146*, 49–68. [CrossRef]
8. Eyre, J.R.; Bell, W.; Cotton, J.; English, S.J.; Forsythe, M.; Healy, S.B.; Pavelin, E.G. Assimilation of satellite data in numerical weather prediction. Part II: Recent years. *Q. J. R. Meteorol. Soc.* **2021**, *148*, 521–556. [CrossRef]
9. Goodberlet, M.A.; Swift, C.T.; Wilkerson, J.C. Remote sensing of ocean surface winds with the special sensor microwave/imager. *J. Geophys. Res. Ocean.* **1989**, *94*, 14547–14555. [CrossRef]
10. Alishouse, J.C.; Snyder, S.A.; Vongsathorn, J.; Ferraro, R.R. Determination of oceanic total precipitable water from the SSM/I. *IEEE Trans. Geosci. Remote Sens.* **1990**, *28*, 811–816. [CrossRef]
11. Bauer, P.; Schuessel, P. Rainfall, total water, ice water, and water vapor over sea from polarized microwave simulations and Special Sensor Microwave/Imager data. *J. Geophys. Res. Atmos.* **1993**, *98*, 20737–20759. [CrossRef]
12. Weng, F.; Grody, N.C.; Ferraro, R.; Basist, A.; Forsyth, D. Cloud Liquid Water Climatology from the Special Sensor Microwave/Imager. *J. Clim.* **1997**, *10*, 1086–1098. [CrossRef]
13. Grody, N.; Zhao, J.; Ferraro, R.; Weng, F.; Boers, R. Determination of precipitable water and cloud liquid water over oceans from the NOAA 15 advanced microwave sounding unit. *J. Geophys. Res. Atmos.* **2001**, *106*, 2943–2953. [CrossRef]

14. Han, Y.; Westwater, E.R. Remote Sensing of Tropospheric Water Vapor and Cloud Liquid Water by Integrated Ground-Based Sensors. *J. Atmos. Ocean. Technol.* **1995**, *12*, 1050–1059. [[CrossRef](#)]
15. Zhao, L.; Weng, F. Retrieval of Ice Cloud Parameters Using the Advanced Microwave Sounding Unit. *J. Appl. Meteorol. Climatol.* **2002**, *41*, 384–395. [[CrossRef](#)]
16. Weng, F.; Zhao, L.; Ferraro, R.R.; Poe, G.; Li, X.; Grody, N.C. Advanced microwave sounding unit cloud and precipitation algorithms. *Radio Sci.* **2003**, *38*, 13. [[CrossRef](#)]
17. Ferraro, R.R.; Weng, F.; Grody, N.C.; Zhao, L.; Meng, H.; Kongoli, C.; Pellegrino, P.; Qiu, S.; Dean, C. NOAA operational hydrological products derived from the advanced microwave sounding unit. *IEEE Trans. Geosci. Remote Sens.* **2005**, *43*, 1036–1049. [[CrossRef](#)]
18. Rosenkranz, P.W. Cloud liquid-water profile retrieval algorithm and validation. *J. Phys. Res.* **2006**, *111*, 1441. [[CrossRef](#)]
19. Liu, Q.; Weng, F. One-dimensional variational retrieval algorithm of temperature, water vapor, and cloud water profiles from advanced microwave sounding unit (AMSU). *IEEE Trans. Geosci. Remote Sens.* **2005**, *43*, 1087–1095. [[CrossRef](#)]
20. Marzano, F.S.; Cimini, D.; Memmo, A.; Montopoli, M.; Rossi, T.; De Sanctis, M.; Lucente, M.; Mortari, D.; Di Michele, S. Flower Constellation of Millimeter-Wave Radiometers for Tropospheric Monitoring at Pseudogeostationary Scale. *IEEE Trans. Geosci. Remote Sens.* **2009**, *47*, 3107–3122. [[CrossRef](#)]
21. Marzano, F.S.; Cimini, D. Flower elliptical-orbit constellation exploiting millimeter-wave radiometry and radio occultation for meteo-climatological applications. *Adv. Geosci.* **2010**, *25*, 167–177. [[CrossRef](#)]
22. Marzano, F.S.; Cimini, D.; Rossi, T.; Mortari, D.; Michele, S.D.; Bauer, P. High-Repetition Millimeter-Wave Passive Remote Sensing of Humidity and Hydrometeor Profiles from Elliptical Orbit Constellations. *J. Appl. Meteorol. Climatol.* **2010**, *49*, 1454–1476. [[CrossRef](#)]
23. Bobylev, L.P.; Zabolotskikh, E.V.; Mitnik, L.M.; Mitnik, M.L. Atmospheric Water Vapor and Cloud Liquid Water Retrieval Over the Arctic Ocean Using Satellite Passive Microwave Sensing. *IEEE Trans. Geosci. Remote Sens.* **2010**, *48*, 283–294. [[CrossRef](#)]
24. Wentz, F.J.; Spencer, R.W. SSM/I Rain Retrievals within a Unified All-Weather Ocean Algorithm. *J. Atmos. Sci.* **1998**, *55*, 1613–1627. [[CrossRef](#)]
25. Sun, N.; Weng, F. Retrieval of Cloud Ice Water Path from Special Sensor Microwave Imager/Sounder (SSMIS). *J. Appl. Meteorol. Climatol.* **2012**, *51*, 366–379. [[CrossRef](#)]
26. Boukabara, S.-A.; Garrett, K.; Grassotti, C.; Iturbide-Sanchez, F.; Chen, W.; Jiang, Z.; Clough, S.A.; Zhan, X.; Liang, P.; Liu, Q.; et al. A physical approach for a simultaneous retrieval of sounding, surface, hydrometeor, and cryospheric parameters from SNPP/ATMS. *J. Geophys. Res. Atmos.* **2013**, *118*, 12600–12619. [[CrossRef](#)]
27. Dong, P.; Weng, F.; Huang, Q.; Han, Y.; Han, W. Estimation of cloud liquid water over oceans from dual oxygen absorption band to support the assimilation of second generation of microwave observation on board the Chinese FY-3 satellite. *Int. J. Remote Sens.* **2017**, *38*, 5003–5021. [[CrossRef](#)]
28. Han, Y.; Yang, J.; Hu, H.; Dong, P. Retrieval of Oceanic Total Precipitable Water Vapor and Cloud Liquid Water from Fengyun-3D Microwave Sounding Instruments. *J. Meteorol. Res.* **2021**, *35*, 371–383. [[CrossRef](#)]
29. Liu, S.; Grassotti, C.; Liu, Q. NOAA Microwave Integrated Retrieval System (MiRS) Cloud Liquid Water Retrieval and Assessment. In Proceedings of the 2018 IEEE 15th Specialist Meeting on Microwave Radiometry and Remote Sensing of the Environment (MicroRad), Cambridge, MA, USA, 27–30 March 2018; pp. 14–19. [[CrossRef](#)]
30. Brath, M.; Fox, S.; Eriksson, P.; Harlow, R.C.; Burgdorf, M.; Buehler, S.A. Retrieval of an ice water path over the ocean from ISMAR and MARSS millimeter and sub-millimeter brightness temperatures. *Atmos. Meas. Tech.* **2018**, *11*, 611–632. [[CrossRef](#)]
31. Blackwell, W.J.; Braun, S.; Bennartz, R.; Velden, C.; DeMaria, M.; Atlas, R.; Dunion, J.; Marks, F.; Rogers, R.; Annane, B.; et al. An overview of the TROPICS NASA Earth Venture Mission. *Q. J. R. Meteorol. Soc.* **2018**, *144* (Suppl. S1), 16–26. [[CrossRef](#)] [[PubMed](#)]
32. Reising, S.C.; Gaier, T.C.; Padmanabhan, S.; Lim, B.H.; Heneghan, C.; Kummerow, C.D.; Berg, W.; Chandrasekar, V.; Radhakrishnan, C.; Brown, S.T.; et al. An Earth Venture In-Space Technology Demonstration Mission for Temporal Experiment for Storms and Tropical Systems (Tempest). In Proceedings of the IGARSS 2018—2018 IEEE International Geoscience and Remote Sensing Symposium, Valencia, Spain, 22–27 July 2018; pp. 6301–6303, ISSN 2153–7003. [[CrossRef](#)]
33. Schulte, R.M.; Kummerow, C.D.; Berg, W.; Reising, S.C.; Brown, S.T.; Gaier, T.C.; Lim, B.H.; Padmanabhan, S. A Passive Microwave Retrieval Algorithm with Minimal View-Angle Bias: Application to the TEMPEST-D CubeSat Mission. *J. Atmos. Ocean. Technol.* **2020**, *37*, 197–210. [[CrossRef](#)]
34. Fritz, S.; Winston, J.S. Synoptic use of radiation measurements from satellite tiros II. *Mon. Weather. Rev.* **1962**, *90*, 1–9. [[CrossRef](#)]
35. Smith, W.L.; Platt, C.M.R. Comparison of Satellite-Deduced Cloud Heights with Indications from Radiosonde and Ground-Based Laser Measurements. *J. Appl. Meteorol. Climatol.* **1978**, *17*, 1796–1802. [[CrossRef](#)]
36. Menzel, W.P.; Smith, W.L.; Stewart, T.R. Improved Cloud Motion Wind Vector and Altitude Assignment Using VAS. *J. Appl. Meteorol. Climatol.* **1983**, *22*, 377–384. [[CrossRef](#)]
37. Eyre, J.R.; Menzel, W.P. Retrieval of Cloud Parameters from Satellite Sounder Data: A Simulation Study. *J. Appl. Meteorol. Climatol.* **1989**, *28*, 267–275. [[CrossRef](#)]

38. Menzel, W.P.; Schmit, T.J.; Wylie, D.P. Cloud characteristics over central Amazonia during GTE/ABLE 2B derived from multispectral visible and infrared spin scan radiometer atmospheric sounder observations. *J. Geophys. Res. Atmos.* **1990**, *95*, 17039–17042. [[CrossRef](#)]
39. Minnis, P.; Liou, K.-N.; Takano, Y. Inference of Cirrus Cloud Properties Using Satellite-observed Visible and Infrared Radiances. Part I: Parameterization of Radiance Fields. *J. Atmos. Sci.* **1993**, *50*, 1279–1304. [[CrossRef](#)]
40. Nakajima, T.; King, M.D. Determination of the Optical Thickness and Effective Particle Radius of Clouds from Reflected Solar Radiation Measurements. Part I: Theory. *J. Atmos. Sci.* **1990**, *47*, 1878–1893. [[CrossRef](#)]
41. King, M.D. Determination of the Scaled Optical Thickness of Clouds from Reflected Solar Radiation Measurements. *J. Atmos. Sci.* **1987**, *44*, 1734–1751. [[CrossRef](#)]
42. Nakajima, T.Y.; Nakajima, T. Wide-Area Determination of Cloud Microphysical Properties from NOAA AVHRR Measurements for FIRE and ASTEX Regions. *J. Atmos. Sci.* **1995**, *52*, 4043–4059. [[CrossRef](#)]
43. Li, J.; Carlson, B.E.; Yung, Y.L.; Lv, D.; Hansen, J.; Penner, J.E.; Liao, H.; Ramaswamy, V.; Kahn, R.A.; Zhang, P.; et al. Scattering and absorbing aerosols in the climate system. *Nat. Rev. Earth. Env.* **2022**, *3*, 363–379. [[CrossRef](#)]
44. Letu, H.; Yang, K.; Nakajima, T.Y.; Ishimoto, H.; Nagao, T.M.; Riedi, J.; Baran, A.J.; Ma, R.; Wang, T.; Shang, H.; et al. High-resolution retrieval of cloud microphysical properties and surface solar radiation using Himawari-8/AHI next-generation geostationary satellite. *Remote Sens. Environ.* **2020**, *239*, 111583. [[CrossRef](#)]
45. Han, Q.; Rossow, W.B.; Lacis, A.A. Near-Global Survey of Effective Droplet Radii in Liquid Water Clouds Using ISCCP Data. *J. Clim.* **1994**, *7*, 465–497. [[CrossRef](#)]
46. Jolivet, D.; Feijt, A.J. Quantification of the accuracy of liquid water path fields derived from NOAA 16 advanced very high resolution radiometer over three ground stations using microwave radiometers. *J. Geophys. Research. Atmos.* **2005**, *110*, D11204. [[CrossRef](#)]
47. Dong, X.; Mace, G.G.; Minnis, P.; Smith, W.L.; Poellot, M.; Marchand, R.T.; Rapp, A.D. Comparison of Stratus Cloud Properties Deduced from Surface, GOES, and Aircraft Data during the March 2000 ARM Cloud IOP. *J. Atmos. Sci.* **2002**, *59*, 3265–3284. [[CrossRef](#)]
48. Brenguier, J.-L.; Pawlowska, H.; Schüller, L.; Preusker, R.; Fischer, J.; Fouquart, Y. Radiative Properties of Boundary Layer Clouds: Droplet Effective Radius versus Number Concentration. *J. Atmos. Sci.* **2000**, *57*, 803–821. [[CrossRef](#)]
49. Schüller, L.; Brenguier, J.-L.; Pawlowska, H. Retrieval of microphysical, geometrical, and radiative properties of marine stratocumulus from remote sensing. *J. Geophys. Res. Atmos.* **2003**, *108*, 8631. [[CrossRef](#)]
50. King, M.D.; Platnick, S.; Yang, P.; Arnold, G.T.; Gray, M.A.; Riedi, J.C.; Ackerman, S.A.; Liou, K.-N. Remote Sensing of Liquid Water and Ice Cloud Optical Thickness and Effective Radius in the Arctic: Application of Airborne Multispectral MAS Data. *J. Atmos. Ocean. Technol.* **2004**, *21*, 857–875. [[CrossRef](#)]
51. Kawamoto, K.; Nakajima, T.; Nakajima, T.Y. A Global Determination of Cloud Microphysics with AVHRR Remote Sensing. *J. Clim.* **2001**, *14*, 2054–2068. [[CrossRef](#)]
52. Roebeling, R.A.; Feijt, A.J.; Stammes, P. Cloud property retrievals for climate monitoring: Implications of differences between Spinning Enhanced Visible and Infrared Imager (SEVIRI) on METEOSAT-8 and Advanced Very High Resolution Radiometer (AVHRR) on NOAA-17. *J. Geophys. Res. Atmos.* **2006**, *111*. [[CrossRef](#)]
53. Pérez, J.C.; Cerdeña, A.; González, A.; Armas, M. Nighttime cloud properties retrieval using MODIS and artificial neural networks. *Adv. Space Res.* **2009**, *43*, 852–858. [[CrossRef](#)]
54. Iwabuchi, H.; Saito, M.; Tokoro, Y.; Putri, N.S.; Sekiguchi, M. Retrieval of radiative and microphysical properties of clouds from multispectral infrared measurements. *Prog. Earth Planet. Sci.* **2016**, *3*, 32. [[CrossRef](#)]
55. Iwabuchi, H.; Putri, N.S.; Saito, M.; Tokoro, Y.; Sekiguchi, M.; Yang, P.; Baum, B.A. Cloud Property Retrieval from Multiband Infrared Measurements by Himawari-8. *J. Meteorol. Soc. Jpn.* **2018**, *96B*, 27–42. [[CrossRef](#)]
56. Hanel, R.A.; Conrath, B.J.; Kunde, V.G.; Prabhakara, C.; Revah, I.; Salomonson, V.V.; Wolford, G. The Nimbus 4 infrared spectroscopy experiment: 1. Calibrated thermal emission spectra. *J. Geophys. Res.* **1972**, *77*, 2629–2641. [[CrossRef](#)]
57. Smith, W.L.; Ma, X.L.; Ackerman, S.A.; Revercomb, H.E.; Knuteson, R.O. Remote Sensing Cloud Properties from High Spectral Resolution Infrared Observations. *J. Atmos. Sci.* **1993**, *50*, 1708–1720. [[CrossRef](#)]
58. Kahn, B.H.; Eldering, A.; Clough, S.A.; Fetzer, E.J.; Fishbein, E.; Gunson, M.R.; Lee, S.-Y.; Lester, P.F.; Realmuto, V.J. Near micron-sized cirrus cloud particles in high-resolution infrared spectra: An orographic case study. *Geophys. Res. Lett.* **2003**, *30*, 1441. [[CrossRef](#)]
59. Huang, H.-L.; Gumley, L.; Strabala, K.; Li, J.; Weisz, E.; Rink, T.; Baggett, K.; Davies, J.; Smith Sr, W.; Dodge, J. International MODIS and AIRS processing package (IMAPP)—A direct broadcast software package for the NASA Earth Observing System. *Bull. Am. Meteorol. Soc.* **2004**, *85*, 159–161. [[CrossRef](#)]
60. Wei, H.; Yang, P.; Li, J.; Baum, B.A.; Huang, H.-L.; Platnick, S.; Hu, Y.; Strow, L. Retrieval of semitransparent ice cloud optical thickness from atmospheric infrared sounder (AIRS) measurements. *IEEE Trans. Geosci. Remote Sens.* **2004**, *42*, 2254–2267. [[CrossRef](#)]

61. Heidinger, A.K.; Pavolonis, M.J. Gazing at cirrus clouds for 25 years through a split window. Part I: Methodology. *J. Appl. Meteorol. Climatol.* **2009**, *48*, 1100–1116. [[CrossRef](#)]
62. Parol, F.; Buriez, J.C.; Brogniez, G.; Fouquart, Y. Information content of AVHRR channels 4 and 5 with respect to the effective radius of cirrus cloud particles. *J. Appl. Meteorol.* **1991**, *30*, 973–984. [[CrossRef](#)]
63. Inoue, T. On the temperature and effective emissivity determination of semi-transparent cirrus clouds by bi-spectral measurements in the 10 μm window region. *J. Meteorol. Soc. Jpn.* **1985**, *63*, 88–99. [[CrossRef](#)]
64. Cooper, S.J.; Garrett, T.J. Identification of small ice cloud particles using passive radiometric observations. *J. Appl. Meteorol. Climatol.* **2010**, *49*, 2334–2347. [[CrossRef](#)]
65. Mitchell, D.L.; d’Entremont, R.P. Satellite retrieval of the liquid water fraction in tropical clouds between -20 and -38 $^{\circ}\text{C}$. *Atmos. Meas. Tech.* **2012**, *5*, 1683–1698. [[CrossRef](#)]
66. Huang, H.-L.; Yang, P.; Wei, H.; Baum, B.A.; Hu, Y.; Antonelli, P.; Ackerman, S.A. Inference of ice cloud properties from high spectral resolution infrared observations. *IEEE Trans. Geosci. Remote Sens.* **2004**, *42*, 842–853. [[CrossRef](#)]
67. Li, J.; Huang, H.-L.; Liu, C.-Y.; Yang, P.; Schmit, T.J.; Wei, H.; Weisz, E.; Guan, L.; Menzel, W.P. Retrieval of Cloud Microphysical Properties from MODIS and AIRS. *J. Appl. Meteorol. Climatol.* **2005**, *44*, 1526–1543. [[CrossRef](#)]
68. Zhou, D.K.; Smith, W.L.; Liu, X.; Larar, A.M.; Mango, S.A.; Huang, H.-L. Physically Retrieving Cloud and Thermodynamic Parameters from Ultraspectral IR Measurements. *J. Atmos. Sci.* **2007**, *64*, 969–982. [[CrossRef](#)]
69. Liu, X.; Zhou, D.K.; Larar, A.M.; Smith, W.L.; Schluessel, P.; Newman, S.M.; Taylor, J.P.; Wu, W. Retrieval of atmospheric profiles and cloud properties from IASI spectra using super-channels. *Atmos. Chem. Phys.* **2009**, *9*, 9121–9142. [[CrossRef](#)]
70. August, T.; Klaes, D.; Schlüssel, P.; Hultberg, T.; Crapeau, M.; Arriaga, A.; O’Carroll, A.; Coppens, D.; Munro, R.; Calbet, X. IASI on Metop-A: Operational Level 2 retrievals after five years in orbit. *J. Quant. Spectrosc. Radiat. Transf.* **2012**, *113*, 1340–1371. [[CrossRef](#)]
71. Martinet, P.; Fourrié, N.; Guidard, V.; Rabier, F.; Montmerle, T.; Brunel, P. Towards the use of microphysical variables for the assimilation of cloud-affected infrared radiances. *Q. J. R. Meteorol. Soc.* **2013**, *139*, 1402–1416. [[CrossRef](#)]
72. Saunders, R.; Hocking, J.; Rayer, P.; Matricardi, M.; Geer, A.; Bormann, N.; Brunel, P.; Karbou, F.; Aires, F. *Rttov-10 Science and Validation Report*; Technical Report No. 1.11; Eumetsat: Darmstadt, Germany, 2012.
73. Martinet, P.; Lavanant, L.; Fourrié, N.; Rabier, F.; Gambacorta, A. Evaluation of a revised IASI channel selection for cloudy retrievals with a focus on the Mediterranean basin. *Q. J. R. Meteorol. Soc.* **2014**, *140*, 1563–1577. [[CrossRef](#)]
74. Rodgers, C.D. *Inverse Methods for Atmospheric Sounding: Theory and Practice. Series on Atmospheric, Oceanic and Planetary Physics*; World Scientific: Singapore, 2000; Volume 2. [[CrossRef](#)]
75. Martinet, P.; Fourrié, N.; Bouteloup, Y.; Bazile, E.; Rabier, F. Toward the improvement of short-range forecasts by the analysis of cloud variables from IASI radiances. *Atmos. Sci. Lett.* **2014**, *15*, 342–347. [[CrossRef](#)]
76. Wu, W.; Liu, X.; Zhou, D.K.; Larar, A.M.; Yang, Q.; Kizer, S.H.; Liu, Q. The Application of PCRTM Physical Retrieval Methodology for IASI Cloudy Scene Analysis. *IEEE Trans. Geosci. Remote Sens.* **2017**, *55*, 5042–5056. [[CrossRef](#)]
77. Feofilov, A.; Stubenrauch, C. *LMD Cloud Retrieval Using IR Sounders. Algorithm Theoretical Basis Document (ATBD) for CIRS-LMD Software Package*, version 2; Institut Pierre Simon Laplace: Guyancourt, France, 2017. [[CrossRef](#)]
78. Khanal, S.; Wang, Z. Uncertainties in MODIS-Based Cloud Liquid Water Path Retrievals at High Latitudes Due to Mixed-Phase Clouds and Cloud-Top Height Inhomogeneity. *J. Geophys. Res. Atmos.* **2018**, *123*, 11154–11172. [[CrossRef](#)]
79. Platnick, S.; Meyer, K.G.; King, M.D.; Wind, G.; Amarasinghe, N.; Marchant, B.; Arnold, G.T.; Zhang, Z.; Hubanks, P.A.; Holz, R.E.; et al. The MODIS Cloud Optical and Microphysical Products: Collection 6 Updates and Examples from Terra and Aqua. *IEEE Trans. Geosci. Remote Sens.* **2017**, *55*, 502–525. [[CrossRef](#)]
80. Menzel, W.P.; Frey, R.A.; Zhang, H.; Wylie, D.P.; Moeller, C.C.; Holz, R.E.; Maddux, B.; Baum, B.A.; Strabala, K.I.; Gumley, L.E. MODIS Global Cloud-Top Pressure and Amount Estimation: Algorithm Description and Results. *J. Appl. Meteorol. Climatol.* **2008**, *47*, 1175–1198. [[CrossRef](#)]
81. Saito, M.; Yang, P.; Huang, X.; Brindley, H.E.; Mlynczak, M.G.; Kahn, B.H. Spaceborne Middle- and Far-Infrared Observations Improving Night-time Ice Cloud Property Retrievals. *Geophys. Res. Lett.* **2020**, *47*, 2020–087491. [[CrossRef](#)]
82. Teng, S.; Liu, C.; Zhang, Z.; Wang, Y.; Sohn, B.-J.; Yung, Y.L. Retrieval of Ice-Over-Water Cloud Microphysical and Optical Properties Using Passive Radiometers. *Geophys. Res. Lett.* **2020**, *47*, 2020–088941. [[CrossRef](#)]
83. Forster, L.; Davis, A.B.; Diner, D.J.; Mayer, B. Toward Cloud Tomography from Space Using MISR and MODIS: Locating the “Veiled Core” in Opaque Convective Clouds. *J. Atmos. Sci.* **2021**, *78*, 155–166. [[CrossRef](#)]
84. Mitra, A.; Loveridge, J.R.; Di Girolamo, L. Fusion of MISR Stereo Cloud Heights and Terra-MODIS Thermal Infrared Radiances to Estimate Two-Layered Cloud Properties. *J. Geophys. Res. Atmos.* **2023**, *128*, 2022–038135. [[CrossRef](#)]
85. Wang, Y.; Yang, P.; Hioki, S.; King, M.D.; Baum, B.A.; Di Girolamo, L.; Fu, D. Ice Cloud Optical Thickness, Effective Radius, and Ice Water Path Inferred from Fused MISR and MODIS Measurements Based on a Pixel-Level Optimal Ice Particle Roughness Model. *J. Geophys. Res. Atmos.* **2019**, *124*, 12126–12140. [[CrossRef](#)]

86. Weisz, E.; Baum, B.A.; Menzel, W.P. Fusion of satellite-based imager and sounder data to construct supplementary high spatial resolution narrowband IR radiances. *J. Appl. Remote Sens.* **2017**, *11*, 036022. [[CrossRef](#)]
87. Leonarski, L.C.; Labonnote, L.; Compiègne, M.; Vidot, J.; Baran, A.J.; Dubuisson, P. Potential of Hyperspectral Thermal Infrared Spaceborne Measurements to Retrieve Ice Cloud Physical Properties: Case Study of IASI and IASI-NG. *Remote Sens.* **2021**, *13*, 116. [[CrossRef](#)]
88. King, M.; Tsay, S.-C.; Platnick, S.; Wang, M.; Liou, K. Cloud Retrieval Algorithms for MODIS: Optical Thickness, Effective Particle Radius, and Thermodynamic Phase. In *MODIS Algorithm Theoretical Basis Document 1997*, No. ATBD-MOD-05; NASA: Washington, DC, USA, 1997.
89. Cox, C.; Munk, W. Statistics of the sea surface derived from sun glitter. *J. Mar. Res.* **1954**, *13*, 198–227.
90. Nakajima, T.; Tanaka, M. Matrix formulations for the transfer of solar radiation in a plane-parallel scattering atmosphere. *J. Quant. Spectrosc. Radiat. Transf.* **1986**, *35*, 13–21. [[CrossRef](#)]
91. Wang, M.; Bailey, S.W. Correction of sun glint contamination on the SeaWiFS ocean and atmosphere products. *Appl. Opt.* **2001**, *40*, 4790–4798. [[CrossRef](#)] [[PubMed](#)]
92. Shi, C.; Nakajima, T. Simultaneous determination of aerosol optical thickness and water-leaving radiance from multispectral measurements in coastal waters. *Atmos. Chem. Phys.* **2018**, *18*, 3865–3884. [[CrossRef](#)]
93. Håkansson, N.; Adok, C.; Thoss, A.; Scheirer, R.; Hörnquist, S. Neural network cloud top pressure and height for MODIS. *Atmos. Meas. Tech.* **2018**, *11*, 3177–3196. [[CrossRef](#)]
94. Strandgren, J.; Bugliaro, L.; Sehnke, F.; Schröder, L. Cirrus cloud retrieval with MSG/SEVIRI using artificial neural networks. *Atmos. Meas. Tech.* **2017**, *10*, 3547–3573. [[CrossRef](#)]
95. Wang, C.; Platnick, S.; Meyer, K.; Zhang, Z.; Zhou, Y. A machine-learning-based cloud detection and thermodynamic-phase classification algorithm using passive spectral observations. *Atmos. Meas. Tech.* **2020**, *13*, 2257–2277. [[CrossRef](#)]
96. Kim, M.; Cermak, J.; Andersen, H.; Fuchs, J.; Stirnberg, R. A New Satellite-Based Retrieval of Low-Cloud Liquid-Water Path Using Machine Learning and Meteosat SEVIRI Data. *Remote Sens.* **2020**, *12*, 3475. [[CrossRef](#)]
97. Min, M.; Li, J.; Wang, F.; Liu, Z.; Menzel, W.P. Retrieval of cloud top properties from advanced geostationary satellite imager measurements based on machine learning algorithms. *Remote Sens. Environ.* **2020**, *239*, 111616. [[CrossRef](#)]
98. Yang, Y.; Sun, W.; Chi, Y.; Yan, X.; Fan, H.; Yang, X.; Ma, Z.; Wang, Q.; Zhao, C. Machine learning-based retrieval of day and night cloud macrophysical parameters over East Asia using Himawari-8 data. *Remote Sens. Environ.* **2022**, *273*, 112971. [[CrossRef](#)]
99. Wang, Q.; Zhou, C.; Zhuge, X.; Liu, C.; Weng, F.; Wang, M. Retrieval of cloud properties from thermal infrared radiometry using convolutional neural network. *Remote Sens. Environ.* **2022**, *278*, 113079. [[CrossRef](#)]
100. Tana, G.; Ri, X.; Shi, C.; Ma, R.; Letu, H.; Xu, J.; Shi, J. Retrieval of cloud microphysical properties from Himawari-8/AHI infrared channels and its application in surface shortwave downward radiation estimation in the sun glint region. *Remote Sens. Environ.* **2023**, *290*, 113548. [[CrossRef](#)]
101. Vinjamuri, K.S.; Vountas, M.; Lelli, L.; Stengel, M.; Shupe, M.D.; Ebell, K.; Burrows, J.P. Validation of the Cloud cci (Cloud Climate Change Initiative) cloud products in the Arctic. *Atmos. Meas. Tech.* **2023**, *16*, 2903–2918. [[CrossRef](#)]
102. Foster, M.J.; Phillips, C.; Heiding, A.K.; Borbas, E.E.; Li, Y.; Menzel, W.P.; Walther, A.; Weisz, E. PATMOS-x Version 6.0: 40 Years of Merged AVHRR and HIRS Global Cloud Data. *J. Clim.* **2023**, *36*, 1143–1160. [[CrossRef](#)]
103. Lin, B.; Minnis, P.; Wielicki, B.; Doelling, D.R.; Palikonda, R.; Young, D.F.; Uttal, T. Estimation of water cloud properties from satellite microwave, infrared and visible measurements in oceanic environments: 2. Results. *J. Geophys. Res. Atmos.* **1998**, *103*, 3887–3905. [[CrossRef](#)]
104. Albrecht, B.A.; Bretherton, C.S.; Johnson, D.; Scubert, W.H.; Frisch, A.S. The Atlantic Stratocumulus Transition Experiment—ASTEX. *Bull. Am. Meteorol. Soc.* **1995**, *76*, 889–904. [[CrossRef](#)]
105. Wilheit, T.T.; Hutchison, K.D. Retrieval of cloud base heights from passive microwave and cloud top temperature data. *IEEE Trans. Geosci. Remote Sens.* **2000**, *38*, 1253–1259. [[CrossRef](#)]
106. Chevallier, F.; Bauer, P.; Mahfouf, J.-F.; Morcrette, J.-J. Variational retrieval of cloud profile from ATOVS observations. *Q. J. R. Meteorol. Soc.* **2002**, *128*, 2511–2525. [[CrossRef](#)]
107. Zhao, L.R.; Grody, N.R.; Ferraro, R.R.; Zou, C.Z.; Weng, F. The New NOAA AMSU hydrological product suite: Validation of AMSU-A TPW and CLW. In *Proceedings of the AMS 10th Conference on Satellite Meteorology and Oceanography*, Long Beach, CA, USA, 9–14 January 2000; pp. 196–199. Available online: <https://ams.confex.com/ams/annual2000/webprogram/Paper6101.html> (accessed on 1 March 2024).
108. Shao, H.; Liu, G. Detecting drizzle in marine warm clouds using combined visible, infrared, and microwave satellite data. *J. Geophys. Res. Atmos.* **2004**, *109*, D07205. [[CrossRef](#)]
109. Huang, J.; Minnis, P.; Lin, B.; Yi, Y.; Fan, T.-F.; Sun-Mack, S.; Ayers, J.K. Determination of ice water path in ice-over-water cloud systems using combined MODIS and AMSR-E measurements. *Geophys. Res. Lett.* **2006**, *33*. [[CrossRef](#)]
110. Romano, F.; Cimini, D.; Rizzi, R.; Cuomo, V. Multilayered cloud parameters retrievals from combined infrared and microwave satellite observations. *J. Geophys. Res. Atmos.* **2007**, *112*, 693–708. [[CrossRef](#)]

111. Holl, G.; Buehler, S.A.; Rydberg, B.; Jiménez, C. Collocating satellite-based radar and radiometer measurements—Methodology and usage examples. *Atmos. Meas. Tech.* **2010**, *3*, 693–708. [[CrossRef](#)]
112. Islam, T.; Srivastava, P.K.; Dai, Q.; Gupta, M. Ice cloud detection from AMSU-A, MHS, and HIRS satellite instruments inferred by cloud profiling radar. *Remote Sens. Lett.* **2014**, *5*, 1012–1021. [[CrossRef](#)]
113. Holl, G.; Eliasson, S.; Mendrok, J.; Buehler, S.A. SPARE-ICE: Synergistic ice water path from passive operational sensors. *J. Geophys. Res. Atmos.* **2014**, *119*, 1504–1523. [[CrossRef](#)]
114. Susskind, J.; Blaisdell, J.M.; Iredell, L. Improved methodology for surface and atmospheric soundings, error estimates, and quality control procedures: The atmospheric infrared sounder science team version-6 retrieval algorithm. *J. Appl. Remote. Sens.* **2014**, *8*, 084994. [[CrossRef](#)]
115. Nalli, N.R.; Barnet, C.D.; Reale, A.; Tobin, D.; Gambacorta, A.; Maddy, E.S.; Joseph, E.; Sun, B.; Borg, L.; Mollner, A.K.; et al. Validation of satellite sounder environmental data records: Application to the Cross-track Infrared Microwave Sounder Suite. *J. Geophys. Res. Atmos.* **2013**, *118*, 13628–13643. [[CrossRef](#)]
116. Marke, T.; Ebell, K.; Löhnert, U.; Turner, D.D. Statistical retrieval of thin liquid cloud microphysical properties using ground-based infrared and microwave observations. *J. Geophys. Res. Atmos.* **2016**, *121*, 14558–14573. [[CrossRef](#)]
117. Smalley, K.M.; Lebsock, M.D. Corrections for Geostationary Cloud Liquid Water Path Using Microwave Imagery. *J. Atmos. Ocean. Technol.* **2023**, *40*, 1049–1061. [[CrossRef](#)]
118. Cimini, D.; Serio, C.; Masiello, G.; Mastro, P.; Ricciardelli, E.; Paola, F.D.; Larosa, S.; Gallucci, D.; Hultberg, T.; August, T.; et al. Spectrum Synergy for Investigating Cloud Microphysics. *Bull. Am. Meteorol. Soc.* **2023**, *104*, 606–622. [[CrossRef](#)]
119. Smith, N.; Barnet, C.D. CLIMCAPS—A NASA Long-Term Product for Infrared + Microwave Atmospheric Soundings. *Earth Space Sci.* **2023**, *10*, 2022–002701. [[CrossRef](#)]
120. Li, S.; Li, X.; Liu, L.; Letu, H.; Hu, S.; Zeng, Q.; Dong, P.; Zhuo, Y. Synergistic Retrievals of Ice Cloud Microphysics by Spaceborne Submillimeter and Infrared Observations. *IEEE Trans. Geosci. Remote Sens.* **2024**, *62*, 4108910. [[CrossRef](#)]
121. Rossow, W.B.; Schiffer, R.A. Advances in Understanding Clouds from ISCCP. *Bull. Am. Meteorol. Soc.* **1999**, *80*, 2261–2288. [[CrossRef](#)]
122. Heidinger, A.K.; Foster, M.J.; Walther, A.; Zhao, X.T. The Pathfinder Atmospheres—Extended AVHRR Climate Dataset. *Bull. Am. Meteorol. Soc.* **2014**, *95*, 909–922. [[CrossRef](#)]
123. Stengel, M.; Stapelberg, S.; Sus, O.; Finkensieper, S.; Würzler, B.; Philipp, D.; Hollmann, R.; Poulsen, C.; Christensen, M.; McGarragh, G. Cloud cci Advanced Very High Resolution Radiometer post meridiem (AVHRR-PM) dataset version 3: 35-year climatology of global cloud and radiation properties. *Earth Syst. Sci. Data* **2020**, *12*, 41–60. [[CrossRef](#)]
124. Karlsson, K.-G.; Johansson, E. On the optimal method for evaluating cloud products from passive satellite imagery using CALIPSO-CALIOP data: Example investigating the CM SAF CLARA-A1 dataset. *Atmos. Meas. Tech.* **2013**, *6*, 1271–1286. [[CrossRef](#)]
125. Karlsson, K.-G.; Anttila, K.; Trentmann, J.; Stengel, M.; Fokke Meirink, J.; Devasthale, A.; Hanschmann, T.; Kothe, S.; Jääskeläinen, E.; Sedlar, J.; et al. CLARA-A2: The second edition of the CM SAF cloud and radiation data record from 34 years of global AVHRR data. *Atmos. Chem. Phys.* **2017**, *17*, 5809–5828. [[CrossRef](#)]
126. Wielicki, B.A.; Barkstrom, B.R.; Harrison, E.F.; Lee, R.B.; Smith, G.L.; Cooper, J.E. Clouds and the Earth’s Radiant Energy System (CERES): An Earth Observing System Experiment. *Bull. Am. Meteorol. Soc.* **1996**, *77*, 853–868. [[CrossRef](#)]
127. Minnis, P.; Sun-Mack, S.; Chen, Y.; Chang, F.-L.; Yost, C.R.; Smith, W.L.; Heck, P.W.; Arduini, R.F.; Bedka, S.T.; Yi, Y.; et al. CERES MODIS Cloud Product Retrievals for Edition 4—Part I: Algorithm Changes. *IEEE Trans. Geosci. Remote Sens.* **2021**, *59*, 2744–2780. [[CrossRef](#)]
128. Marquardt, D.W. An Algorithm for Least-Squares Estimation of Nonlinear Parameters. *J. Soc. Ind. Appl. Math.* **1963**, *11*, 431–441. [[CrossRef](#)]
129. Aires, F.; Prigent, C.; Rossow, W.B.; Rothstein, M. A new neural network approach including first guess for retrieval of atmospheric water vapor, cloud liquid water path, surface temperature, and emissivities over land from satellite microwave observations. *J. Geophys. Res. Atmos.* **2001**, *106*, 14887–14907. [[CrossRef](#)]
130. Blackwell, W.J. A neural-network technique for the retrieval of atmospheric temperature and moisture profiles from high spectral resolution sounding data. *IEEE Trans. Geosci. Remote Sens.* **2005**, *43*, 2535–2546. [[CrossRef](#)]
131. Aires, F.; Aznay, O.; Prigent, C.; Paul, M.; Bernardo, F. Synergistic multi-wavelength remote sensing versus a posteriori combination of retrieved products: Application for the retrieval of atmospheric profiles using MetOp-A. *J. Geophys. Res. Atmos.* **2012**, *117*, D18304. [[CrossRef](#)]
132. Pavolonis, M.J.; Heidinger, A.K.; Uttal, T. Daytime Global Cloud Typing from AVHRR and VIIRS: Algorithm Description, Validation, and Comparisons. *J. Appl. Meteorol. Climatol.* **2005**, *44*, 804–826. [[CrossRef](#)]
133. Marchant, B.; Platnick, S.; Meyer, K.; Arnold, G.T.; Riedi, J. MODIS Collection 6 shortwave-derived cloud phase classification algorithm and comparisons with CALIOP. *Atmos. Meas. Tech.* **2016**, *9*, 1587–1599. [[CrossRef](#)] [[PubMed](#)]

134. Baum, B.A.; Menzel, W.P.; Frey, R.A.; Tobin, D.C.; Holz, R.E.; Ackerman, S.A.; Heidinger, A.K.; Yang, P. MODIS Cloud-Top Property Refinements for Collection 6. *J. Appl. Meteorol. Climatol.* **2012**, *51*, 1145–1163. [[CrossRef](#)]
135. Walther, A.; Heidinger, A.K. Implementation of the Daytime Cloud Optical and Microphysical Properties Algorithm (DCOMP) in PATMOS-x. *J. Appl. Meteorol. Climatol.* **2012**, *51*, 1371–1390. [[CrossRef](#)]

Disclaimer/Publisher’s Note: The statements, opinions and data contained in all publications are solely those of the individual author(s) and contributor(s) and not of MDPI and/or the editor(s). MDPI and/or the editor(s) disclaim responsibility for any injury to people or property resulting from any ideas, methods, instructions or products referred to in the content.